Molecular Cell

Article

The E3 ligase RNF32 controls the IκB kinase complex and NF-κB signaling in intestinal stem cells

Graphical abstract

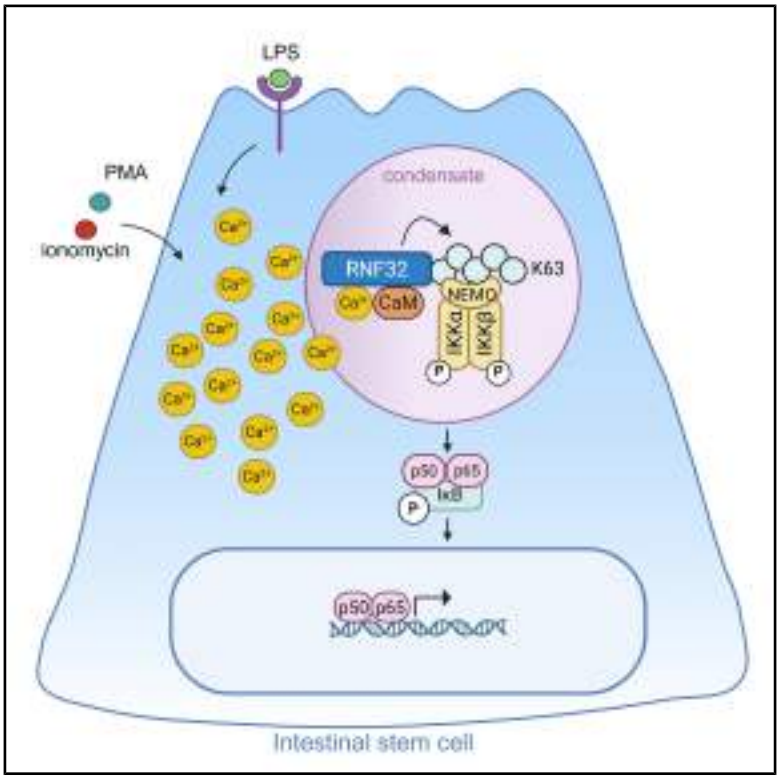

Highlights

- RNF32 is a Ca^{2+}-calmodulin-dependent E3 ubiquitin ligase
- Polyubiquitin chains conjugated to RNF32 recruit and activate the IκB kinase complex
- Ca^{2+} rise triggers RNF32 phase separation needed for the formation of NEMO condensates
- RNF32 regulates the NF-κB signaling pathway in intestinal stem cells

Authors

Angela Lauriola, Juliana Haydeé Enriqué Steinberg, Motoharu Sarubo, ..., Spartaco Santi, Yasusei Kudo, Daniele Guardavaccaro

Correspondence

yasusei@tokushima-u.ac.jp (Y.K.), daniele.guardavaccaro@univr.it (D.G.)

In brief

Lauriola, Enriqué Steinberg, et al. report that RNF32, a ubiquitin ligase enriched in intestinal stem cells, links calcium levels to NF-κB signaling by activating the IKK complex. This study uncovers a calcium-dependent mechanism involved in responses to bacterial stimuli, revealing how intestinal cells integrate signaling cues to regulate intestinal homeostasis.

Lauriola et al., 2025, Molecular Cell *85*, 4254–4267
November 20, 2025
https://doi.org/10.1016/j.molcel.2025.10.005

CellPress

CellPress
OPEN ACCESS

Molecular Cell

Article

The E3 ligase RNF32 controls the IκB kinase complex and NF-κB signaling in intestinal stem cells

Angela Lauriola,[1,9] Juliana Haydeé Enriqué Steinberg,[1,9] Motoharu Sarubo,[2] Elena Maspero,[3] Fabiana Alejandra Rossi,[4,5] Yasuhiro Mouri,[2] Marco Pedretti,[1] Mohsen Hajisadeghian,[1] Vincenzo Taibi,[3] Andrea Vettori,[1] Nicola Vitulo,[1] Michael Assfalg,[1] Mariapina D'Onofrio,[1] Mario Rossi,[4,5] Akihiro Yasue,[6] Alessandra Astegno,[1] Simona Polo,[3] Spartaco Santi,[7] Yasusei Kudo,[2,8,*] and Daniele Guardavaccaro[1,10,*]

[1]Department of Biotechnology, University of Verona, 37134 Verona, Italy
[2]Department of Oral Bioscience, Tokushima University, 3-18-15 Kuramoto, Tokushima 770-8504, Japan
[3]IFOM ETS, The AIRC Institute of Molecular Oncology, 20139 Milan, Italy
[4]Instituto de Investigaciones en Medicina Traslacional (IIMT), CONICET, Universidad Austral, B1629AHJ Pilar, Argentina
[5]Facultad de Ciencias Biomédicas, Universidad Austral, B1629AHJ Pilar, Argentina
[6]Nakano-Cho niconicoKamKam Dental and Orthodontics, 1-31 Nakano-cho, Tokushima 770-0932, Japan
[7]Consiglio Nazionale delle Ricerche (CNR) Institute of Molecular Genetics "Luigi Luca Cavalli-Sforza", 40136 Bologna, Italy
[8]Institute of Photonics and Human Health Frontier, Tokushima University, 3-18-15 Kuramoto, Tokushima 770-8504, Japan
[9]These authors contributed equally
[10]Lead contact
*Correspondence: yasusei@tokushima-u.ac.jp (Y.K.), daniele.guardavaccaro@univr.it (D.G.)
https://doi.org/10.1016/j.molcel.2025.10.005

SUMMARY

Nuclear factor κB (NF-κB) signaling is a central pathway regulating a plethora of cellular functions. Here, we find that RNF32, a RING E3 ubiquitin ligase whose expression is enriched in murine intestinal stem cells, regulates the activity of the IκB kinase (IKK) complex, the signal integration hub for NF-κB activation. The E3 ligase activity of RNF32 depends on calmodulin, the primary calcium sensor in eukaryotic cells. Increased levels of intracellular calcium ion (Ca^{2+}) induce RNF32 binding to calmodulin, RNF32 activation, and autoubiquitylation. In turn, polyubiquitin chains conjugated to RNF32 recruit NEMO, the regulatory subunit of the IKK complex. Moreover, Ca^{2+} rise triggers RNF32 phase separation, which is required for the formation of NEMO condensates and IKK activation. Finally, we show that RNF32 is required for NF-κB activation triggered by bacterial lipopolysaccharides. Collectively, our findings uncover a mechanism controlling NF-κB signaling in the intestinal epithelium.

INTRODUCTION

In adult organisms, multiple tissues are continuously regenerated by resident stem cells. The intestinal epithelium is a highly regenerative tissue, as it renews itself every 4–5 days.[1] Although intestinal villi constantly shed differentiated cells into the gut lumen, adult stem cells residing at the bottom of intestinal crypts efficiently maintain a suitably sized and diversified cell population for tissue homeostasis in steady-state conditions or for regeneration following tissue damage. Although recent reports have demonstrated that nutrients and environmental factors affect stem cell behavior,[2] our understanding of the underlying molecular mechanisms and the regulatory events is still limited.

Dimeric nuclear factor κB (NF-κB) transcription factors coordinate gene expression programs to control multiple key cellular functions.[3,4] In unstimulated cells, NF-κB dimers are sequestered in the cytoplasm by an inhibitory protein of the IκB family.[5,6] In response to a great diversity of stimuli, which include endogenous and exogenous ligands as well as many physical and chemical stresses, IκBs are phosphorylated by the IκB kinase (IKK) complex, polyubiquitylated by the $SCF^{\beta TrCP}$ ubiquitin ligase, and degraded by the proteasome.[7] IκB proteolysis frees NF-κB dimers, which translocate into the nucleus, where they drive the expression of a plethora of genes implicated in diverse cellular processes.[5] Despite recent biochemical, genetic, and structural data having provided important insights into IKK structure, function, and regulation, including the crucial role of several types of polyubiquitylation chains,[6,8] our knowledge of how different stimuli specifically converge into IKK activation is still incomplete.

Here, we identify RNF32, an uncharacterized RING-type E3 ubiquitin ligase specifically expressed in intestinal stem cells (ISCs), as a regulator of the IKK complex and NF-κB signaling. We show that the ligase activity of RNF32 depends on Ca^{2+} and calmodulin (CaM), which stimulate the Lys63-linked autoubiquitylation of RNF32 and recruitment of NEMO via its ubiquitin-binding domains. RNF32 is required for NF-κB signaling activation upon stimuli, such as bacterial lipopolysaccharides (LPSs), that result in increased levels of intracellular Ca^{2+}.

RESULTS

Expression profile of E3 ubiquitin ligases in ISCs

To uncover additional roles of ubiquitylation in the regulation of intestinal epithelium homeostasis, we mined gene expression profile data of murine ISCs. Koo and colleagues sorted intestinal crypt cells based on the expression of LGR5 (leucine-rich repeat-containing G-protein-coupled receptor 5), a well-established adult stem cell marker of the intestinal epithelium,[9] and conducted genome-wide transcription profiling.[10] We focused our attention on the gene expression profile of 655 E3 ubiquitin ligases belonging to various E3 classes (Figure S1A) and found that the expression of several E3s is enriched in LGR5-positive intestinal crypt cells (Figure S1B). Among them, RNF32, a poorly characterized RING ubiquitin ligase, displays an expression profile similar to well-known ISC genes (Figure 1A). Analysis of additional transcriptional profiling databases confirmed that RNF32 expression is enriched in LGR5-positive ISCs.[11] To validate that RNF32 is expressed in ISCs, we performed *in situ* hybridization of murine intestinal and colonic epithelia. We found that the RNF32 mRNA is mainly expressed at the base of intestinal and colonic crypts where stem cells reside (Figure 1B).

Interestingly, TCGA (The Cancer Genome Atlas Program) human cancer transcriptomic RNA sequencing (RNA-seq) and microarray data indicate that expression of RNF32 is elevated mainly in primary colorectal tumors (Figures S2A–S2F). When RNF32 expression is dichotomized into low versus high expression groups of colorectal cancer patients, a significant association between high RNF32 expression and decreased overall survival (OS) was observed (Figure S2G). Moreover, a multivariate analysis of OS adjusted for other prognostic factors revealed that $RNF32^{High}$ is an independent prognostic predictor in patients with colon cancer (Figure S2H).

RNF32 is a Ca^{2+}-CaM-dependent E3 ubiquitin ligase

RNF32 contains two evolutionarily conserved RING domains[12] and one IQ (Ile193-Gln194) motif,[13,14] an amphiphilic seven-turn α-helix present in CaM binding proteins (Figure 1C). To identify RNF32 interactors, we carried out mass spectrometry analysis of RNF32 immunocomplexes purified from HEK293T cells. CaM was the most represented protein recovered in the RNF32 immunocomplex (Figure 1D). The RNF32-CaM interaction in cultured cells was confirmed by affinity purification of His-tagged CaM followed by immunoblotting (Figure 1E). Moreover, immunoprecipitation of FLAG-tagged RNF32 followed by immunoblotting demonstrated that wild-type RNF32, but not the RNF32(I193E/Q194A) mutant (RNF32-IQ_m), coimmunoprecipitated with CaM (Figure 1F). Treatment of cells with thapsigargin, an inhibitor of the sarco/endoplasmic reticulum Ca^{2+} ATPase pumps that increases cytosolic calcium levels, stimulated RNF32 binding to CaM (Figure 1G). Accordingly, *in vitro* translated RNF32 interacted with purified recombinant CaM only in the presence of $CaCl_2$ (Figure 1H). Moreover, the RNF32-CaM binding was prevented by EGTA, a calcium ion chelator (Figure S3A).

We then examined the ability of a synthetic peptide (RNF32p) encompassing the IQ domain of RNF32 (^{188}KCVTRIQAYWRGCV VRKWYRNLR^{210}) (Figure S3B) to bind purified recombinant CaM. Complex formation between RNF32p and CaM was first demonstrated through gel shift experiments (Figure S3C). Incubating RNF32p with CaM in the presence of Ca^{2+} resulted in the appearance of a slower-migrating band likely representing the CaM-RNF32p complex and the disappearance of the free Ca^{2+}-CaM band. Since CaM lacks tryptophan residues, we utilized Trp fluorescence in RNF32p to directly monitor peptide binding to CaM. The Trp indole ring emission is environment-sensitive, emitting around 355 nm in water but showing a blue shift and increased intensity when buried in a hydrophobic region upon binding to CaM. Adding CaM to RNF32p in the presence of Ca^{2+} resulted in increased fluorescence quantum yield and a 22 nm blue shift (Figure S3D), confirming the binding of RNF32p to Ca^{2+}-CaM.

Next, we characterized the ubiquitin ligase activity of RNF32 in cultured cells. Wild-type RNF32, but not the RNF32(C127A/C130A/C293A/C296A) mutant (RNF32-$R1R2_m$) in which the conserved cysteine residues within each of the two RING domains have been replaced by alanine, displayed autoubiquitylation activity (Figure 1I). Moreover, the RNF32-IQ_m mutant, which is unable to bind CaM, displayed reduced autoubiquitylation when compared with wild-type RNF32. To rule out that mutations in the zinc-binding cysteine residues may perturb the overall RING domain structures, we mutated the conserved isoleucine residue that is known to mediate E2 binding in other RING E3 ubiquitin ligases.[12] The RNF32 (I129A/I295A) mutant, in which both Iso129 (in RING1) and Iso295 (in RING2) were replaced by alanine, displayed decreased binding to UBCH5 (Figure S3E) and ubiquitylation (Figure S3F) when compared with wild-type RNF32. These results demonstrate that efficient synthesis of polyubiquitin chains by RNF32 requires intact RING and IQ domains. In agreement with these experiments carried out in cultured cells, *in vitro* ubiquitylation reactions demonstrated that purified recombinant CaM stimulates, and the RNF32 RING domains are indispensable for, RNF32 ligase activity (Figures 1J and S3G).

To rule out that CaM is a substrate of RNF32, we examined whether RNF32 promotes CaM ubiquitylation in cultured cells. As shown in Figure S3H, ectopic expression of RNF32 does not induce CaM ubiquitylation. Moreover, immunopurified RNF32 does not promote CaM ubiquitylation *in vitro* (Figure S3I). Finally, mass spectrometry analysis of the RNF32-bound CaM did not reveal CaM ubiquitylation, whereas RNF32 is highly modified by ubiquitin (Table S1). These results suggest that CaM is not a substrate of RNF32. Rather, it is a regulator controlling RNF32 activity in response to an increase in intracellular calcium.

RNF32 interacts with the IKK complex and controls NF-κB signaling

Mass spectrometry analysis of endogenous proteins copurifying with FLAG-tagged RNF32 revealed the presence of IKKα, IKKβ, and IKKγ/NEMO (Figure 1D), components of the IKK complex that controls nuclear factor kappa B (NF-κB) signaling.[3,4] The interaction of ectopically expressed FLAG-HA-tagged RNF32 with endogenous IKKα, IKKβ, and IKKγ/NEMO was confirmed by coimmunoprecipitation (Figure 2A). Notably, the inactive RNF32-$R1R2_m$ and RNF32-IQ_m mutants, which display a defective ubiquitylation activity (Figure 1I), did not coimmunoprecipitate with IKKα, IKKβ, and IKKγ/NEMO (Figure 2B), suggesting that the IKK complex may associate with RNF32 via its self-ligated polyubiquitin chains. Indeed, NEMO, the regulatory subunit of the IKK complex,

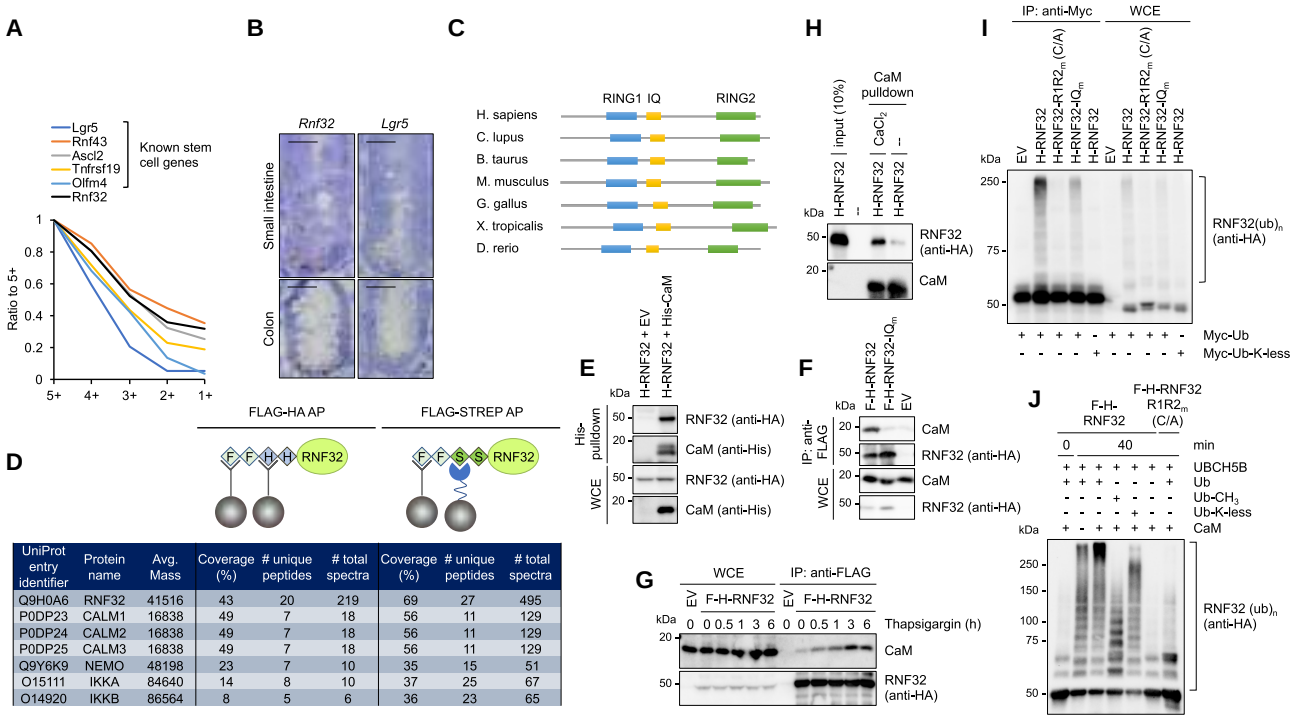

UniProt entry identifier	Protein name	Avg. Mass	Coverage (%)	# unique peptides	# total spectra	Coverage (%)	# unique peptides	# total spectra
Q9H0A6	RNF32	41516	43	20	219	69	27	495
P0DP23	CALM1	16838	49	7	18	56	11	129
P0DP24	CALM2	16838	49	7	18	56	11	129
P0DP25	CALM3	16838	49	7	18	56	11	129
Q9Y6K9	NEMO	48198	23	7	10	35	15	51
O15111	IKKA	84640	14	8	10	37	25	67
O14920	IKKB	86564	8	5	6	36	23	65

Figure 1. RNF32 is a Ca^{2+}-CaM-dependent ubiquitin ligase expressed in ISCs

(A) Graph of the expression profile of RNF32 and known stem cell genes. Crypt cells were sorted on the basis of LGR5-GFP expression into five fractions (highest in fraction 5+), and microarray expression profiling was performed.[10] Each sample was compared with sample 5+.

(B) *In situ* hybridization showing Rnf32 and Lgr5 expression in the mouse small intestine (top) and colon (bottom). Scale bar, 20 μm.

(C) Schematic representation of RNF32 orthologs with the indicated domains.

(D) Identification of RNF32 interactors by affinity purification and mass spectrometry analysis as described in STAR Methods.

(E) HEK293T cells were transfected with HA-tagged RNF32 and either His-tagged CaM or an empty vector (EV). Whole-cell extracts (WCEs) were subjected to nickel-IMAC (immobilized metal affinity chromatography) affinity purification. Purified complexes were analyzed by immunoblotting.

(F) HEK293T cells were transfected with an EV, FLAG-HA-tagged wild-type (WT) RNF32, or the RNF32(I193E/Q194A) mutant (RNF32-IQ_m). WCEs were subjected to immunoprecipitation using anti-FLAG resin. Immunocomplexes were analyzed by immunoblotting.

(G) HEK293T cells were transfected with an EV or FLAG-HA-tagged WT RNF32 and treated with thapsigargin. WCEs were subjected to immunoprecipitation using anti-FLAG resin. Immunocomplexes were analyzed by immunoblotting.

(H) HA-RNF32 was transcribed/translated *in vitro* and incubated with Sepharose-4B beads coupled to human CaM with or without $CaCl_2$. After washing, the beads were analyzed by immunoblotting.

(I) HEK293T cells were transfected with FLAG-HA-tagged WT RNF32, RNF32(C127A/C130A/C293A/C296A) (RNF32-R1R2$_m$ C/A), RNF32(I193E/Q194A) (RNF32-IQ_m), or an EV together with MYC-tagged ubiquitin (WT or lysine-less [K-less]). Cells were lysed, and the bulk of ubiquitylated proteins was immunoprecipitated with an anti-MYC antibody. Immunoprecipitates were analyzed by immunoblotting.

(J) *In vitro* ubiquitin ligation assay of immunopurified FLAG-HA-tagged RNF32 (WT or RNF32-R1R2$_m$ C/A) was carried out in the presence of purified recombinant E1, UBCH5B (E2), with or without purified recombinant CaM, WT ubiquitin, Lys-less (K-less), or methylated ubiquitin (Ub-CH_3) as indicated. Samples were resolved by SDS-PAGE and probed with anti-HA antibodies.

See also Figures S1, S2, and S3.

has been shown to interact with polyubiquitin chains via its ubiquitin-binding domain.[7] As shown in Figure 2C, the NEMO (F312A) mutant defective for ubiquitin binding[15–17] failed to coimmunoprecipitate with wild-type RNF32.

Next, we asked whether RNF32 controls NF-κB signaling. We generated RNF32$^{-/-}$ HCT116 cells by CRISPR genome editing (Figures S4A–S4D) and examined NF-κB signaling by assessing phosphorylation and degradation of its cytoplasmic inhibitor IκBα as well as the activating phosphorylation of IKKα and IKKβ in response to several stimuli. RNF32 seemed to be dispensable for the activation of NF-κB signaling in response to the inflammatory cytokines tumor necrosis factor alpha (TNF-α) (Figures S4E–S4G) and interleukin (IL)-1β (Figure S4H). However, cell treatment with the Ca^{2+} ionophore ionomycin (IO) in conjunction with the phorbol ester 12-myristate 13-acetate (PMA), which are known to increase intracellular Ca^{2+} levels (Figure 2D) and induce NF-κB signaling in a variety of cells, failed to activate NF-κB signaling in RNF32-deficient cells (Figure 2E). Moreover, RNF32 was required for the expression of an NF-κB luciferase reporter in response to IO and PMA (Figure 2F). Rescue experiments, in which the expression of RNF32 was reconstituted by lentiviral transduction of RNF32$^{-/-}$ HCT116 cells, demonstrated that wild-type RNF32, but not the RNF32-R1R2$_m$ or RNF32-IQ_m mutant, stimulated the expression of the NF-κB reporter (Figure 2G). Next, we examined

CellPress
OPEN ACCESS

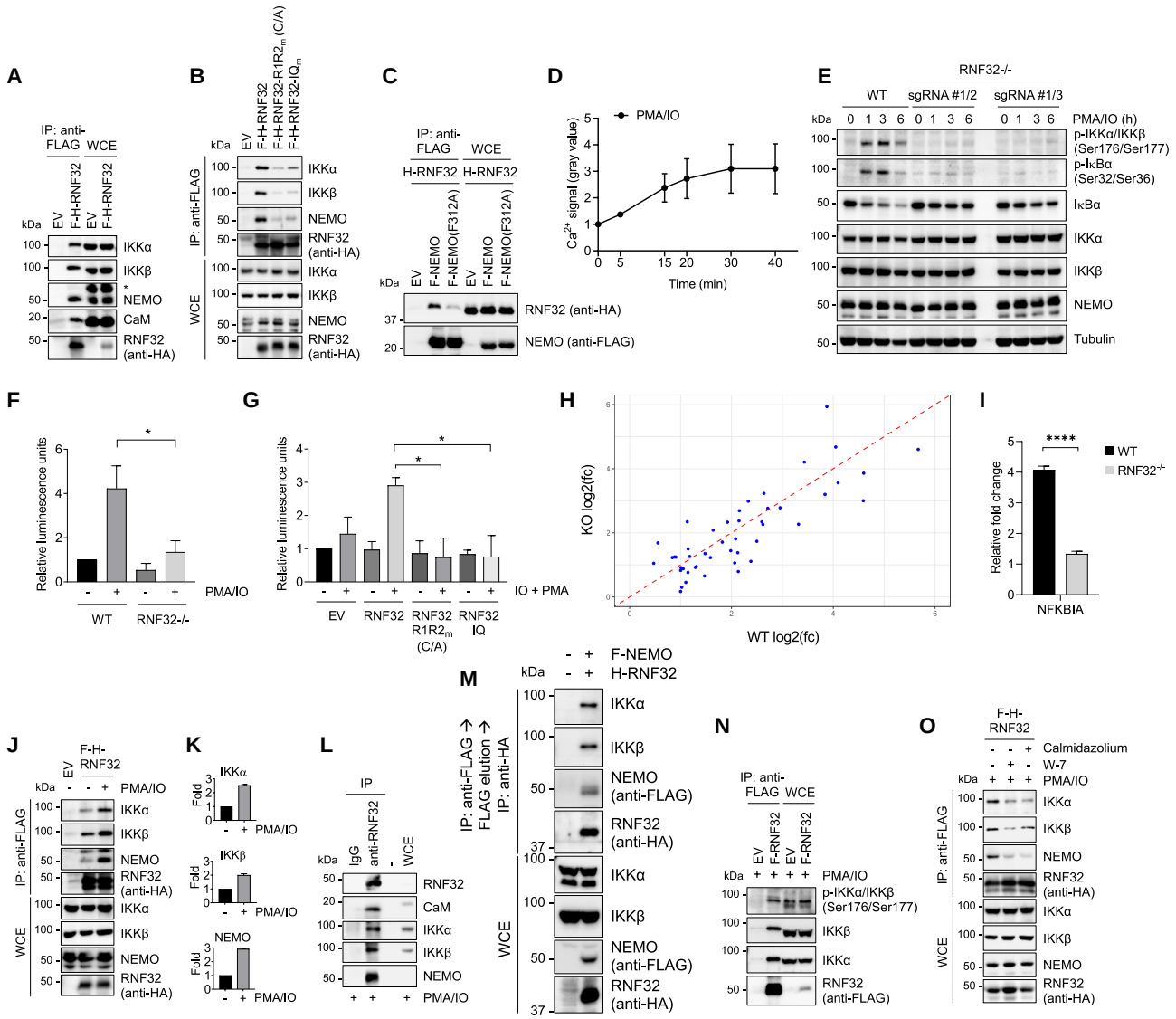

Figure 2. RNF32 interacts with the IKK complex and is required for NF-κB signaling activation

(A) FLAG-HA-tagged RNF32 was expressed in HEK293T cells and immunoprecipitated (IP). FLAG-RNF32 immunocomplexes were analyzed by immunoblotting.

(B) HEK293T cells were transfected with FLAG-HA-tagged WT RNF32, the RNF32(C127A/C130A/C293A/C296A) mutant (RNF32-R1R2$_m$), the RNF32(I193E/Q194A) mutant (RNF32-IQ$_m$), or an empty vector (EV). Whole-cell extracts (WCE) were then IP with anti-FLAG resin. Immunocomplexes were analyzed by immunoblotting.

(C) HEK293T cells were transfected with an EV, FLAG-tagged NEMO (WT or the F312A mutant), and HA-tagged RNF32. WCEs were IP with anti-FLAG resin, and immunocomplexes were analyzed by immunoblotting.

(D) HCT116 cells were treated with the live cell red fluorescent calcium indicator Biotracker 609 Red Ca^{2+} AM Dye and stimulated with 10 ng/ml phorbol-12-myristate-13-acetate (PMA) and 950 nM ionomycin (IO) for the indicated times. The probe fluorescence intensity was measured by fluorescence microscopy. The mean ± SEM (n = 10 cells) is shown.

(E) Parental or RNF32$^{-/-}$ HCT116 cells (two different clones: sgRNA (single-guide RNA) #1/2 and sgRNA #1/3) were treated with PMA and IO for the indicated times. Cells were lysed, and WCEs were analyzed by immunoblotting.

(F) Parental or RNF32$^{-/-}$ HCT116 cells were transfected with a luciferase reporter linked to an NF-κB response element (pNF-κB-luc) and treated as in (E) for 6 h. Cells were collected, and the relative luciferase signal was quantified. The value given for luciferase activity in untreated WT cells was set at 1. Means ± SEM (n = 3) *p < 0.05, unpaired Student's t test.

(G) Parental or RNF32$^{-/-}$ HCT116 cells re-expressing RNF32 (WT or mutants) were transfected with a luciferase reporter linked to an NF-κB response element and treated as in (F). Cells were collected, and the relative luciferase signal was quantified as in (F). Means ± SEM (n = 3) *p < 0.05, unpaired Student's t test.

(H) Scatter plot of transcriptome-wide $\log_2$ fold changes between RNF32$^{-/-}$ and WT cells treated with PMA and IO for 90 min. Each dot represents a single NF-κB target gene. Gene expression was quantified by RNA-seq and normalized to TPM. A linear regression line (red) with a 95% confidence interval is shown. The observed correlation (R^2 = 0.7457, p < 0.0001) indicates consistent transcriptomic trends across conditions.

(legend continued on next page)

whether RNF32 deficiency affects the NF-κB transcriptional program. We analyzed differential gene expression in wild-type and RNF32$^{-/-}$ HCT116 cells upon treatment with PMA and IO by RNA-seq. We found that the expression of 621 genes is altered in stimulated RNF32-deficient cells when compared with wild-type cells. Of these, 48 are known NF-κB target genes (Figure 2H; Table S2). The defective upregulation of the NF-κB target gene NFKBIA (nuclear factor of kappa light polypeptide gene enhancer in B-cells inhibitor, alpha) in RNF32 knockout cells was confirmed by qRT-PCR (Figure 2I). Notably, the treatment of cells with IO and PMA stimulated the interaction of RNF32 with the exogenous and endogenous IKK complex (Figures 2J–2M). The RNF32-bound IKK complex was active, as shown by its phosphorylation on Ser176 and Ser177 of IKKα and IKKβ, respectively (Figure 2N). Furthermore, the CaM inhibitors W-7 and Calmidazolium reduced the binding of RNF32 to the IKK complex in cells treated with PMA and IO (Figure 2O).

Modulation of RNF32 expression does not affect the levels of intracellular calcium in untreated cells or the kinetics of calcium increase upon treatment with PMA and IO (Figures S4I–S4L), excluding the possibility that RNF32 might regulate intracellular calcium levels and thus indirectly control NF-κB activity. To rule out that RNF32 may mediate ubiquitin conjugation of the IKKs, we modulated RNF32 expression in cultured cells and examined IKKα, IKKβ, or IKKγ/NEMO ubiquitylation and stability. As shown in Figures S4M–S4O, overexpression or silencing of RNF32 does not affect IKKα, IKKβ, or IKKγ/NEMO polyubiquitylation and turnover. Altogether, these results indicate that RNF32 is essential for NF-κB signaling activation in response to IO and PMA and that this function is mediated by the Ca^{2+}/CaM-dependent autoubiquitylation activity of RNF32.

RNF32 forms liquid-like condensates and is required for liquid phase separation of NEMO in stimulated cells

As liquid phase separation triggered by polyubiquitin chains is involved in NF-κB activation,[17] we wondered whether RNF32 forms liquid-like condensates. Both endogenous and ectopically expressed RNF32, but not the inactive RNF32-R1R2$_m$ and RNF32-IQ$_m$ mutants, formed cytoplasmic puncta in cells stimulated with IO and PMA (Figures 3A–3F and S5A–S5D). However, the total abundance of RNF32 did not change remarkably in response to IO and PMA treatment either at the protein level (Figure 2J) or at the mRNA level (Figure S5E). RNF32 cytoplasmic puncta did not require *de novo* protein synthesis and likely resulted from RNF32 redistribution, as they still formed in the presence of the translation elongation inhibitor cycloheximide (Figures S5F and S5G). To analyze the dynamics of RNF32 puncta, we carried out live-imaging experiments in U2OS cells expressing near-endogenous levels of GFP-tagged RNF32. We found that highly dynamic RNF32 puncta formed within 90 min after stimulation with IO and PMA (Figures 3G and 3H). Holotomography microscopy revealed that the cytoplasmic puncta labeled with GFP-RNF32 do not display characteristics indicative of membrane-bound organelles (Figure S5H). The RNF32 cytoplasmic puncta displayed liquid-like features, as demonstrated by fluorescence recovery after photobleaching (FRAP) (Figures 3I and 3J). In cells treated with IO and PMA, RNF32 condensates recovered 40–60 s after photobleaching. Moreover, treating cells with IO and PMA stimulated GFP-RNF32 colocalization with mCherry-NEMO (Figures 3K–3N), IKKα (Figures S5I and S5J), IKKβ (Figures S5K and S5L), linkage-specific ubiquitin chains (Figures S5M–S5O), and CaM (Figures S5P and S5Q). In addition, the CaM inhibitor W-7 greatly reduced the formation of RNF32 condensates (Figures S5R and S5S). Notably, IO and PMA induced the formation of NEMO condensates in parental cells but not in RNF32-deficient cells (Figures 3C and 3D). These results indicate that RNF32 forms liquid-like condensates, where it partially colocalizes with NEMO, IKKα, IKKβ, ubiquitin, and CaM, and is essential for liquid phase separation of NEMO in stimulated cells.

Characterization of RNF32-dependent ubiquitylation

Different types of polyubiquitin chains have been implicated in the activation of the IKK complex.[6,8] Mass spectrometry analysis of immunopurified RNF32 suggested that the polyubiquitin chains conjugated onto RNF32 are linked through ubiquitin Lys48 and Lys63 (Figure 4A). The absence of peptides spanning the N and C termini of ubiquitin suggested that RNF32 is not modified by linear ubiquitylation. Lys48- and Lys63-linked polyubiquitylation of RNF32 was confirmed by experiments in which RNF32 was expressed in cells along with wild-type ubiquitin, the Lys-less ubiquitin mutant, or ubiquitin carrying point mutations in the Lys48 or Lys63 site of isopeptide linkage (K48R and K63R). As shown in Figure 4B, RNF32 autoubiquitylation in cells expressing the K48R and K63R ubiquitin mutants was decreased

(I) Relative mRNA expression levels of NFKBIA, a well-known NF-κB target gene, were measured by quantitative real-time PCR. Expression levels are shown as fold change in RNF32$^{-/-}$ cells compared with WT cells, either untreated or treated as in (H). Data were normalized to RPLP0 and are presented as mean ± SEM (n = 3). *p < 0.05 unpaired two-tailed Student's t test.

(J) RNF32$^{-/-}$ HCT116 cells re-expressing WT RNF32 were treated with PMA and IO as in (H). FLAG-RNF32 was IP with an anti-FLAG resin and analyzed by immunoblotting.

(K) The graphs represent the quantification of IKKα (top), IKKβ (middle), or NEMO (bottom) coimmunoprecipitated with RNF32 as shown in (J). The value given for each kinase coimmunoprecipitated with RNF32 in untreated cells was set at 1. Means ± SEM (n = 3).

(L) WCEs from HEK293T cells treated with PMA and IO for 90 min were IP with an anti-RNF32 antibody. RNF32 immunocomplexes were then analyzed by immunoblotting.

(M) HEK293T cells were transfected with HA-tagged RNF32 and FLAG-tagged NEMO. WCEs were IP with anti-FLAG resin, and immunocomplexes were eluted and re-IP with an anti-HA antibody followed by immunoblotting.

(N) HEK293T cells expressing FLAG-tagged WT RNF32 were treated as in (L). WCEs were IP with an anti-FLAG resin. Immunocomplexes and WCEs were analyzed by immunoblotting.

(O) HEK293T cells expressing FLAG-tagged RNF32 were treated as in (N) with or without the indicated CaM inhibitors W-7 or calmidazolium. WCEs were analyzed as in (N).

See also Figure S4.

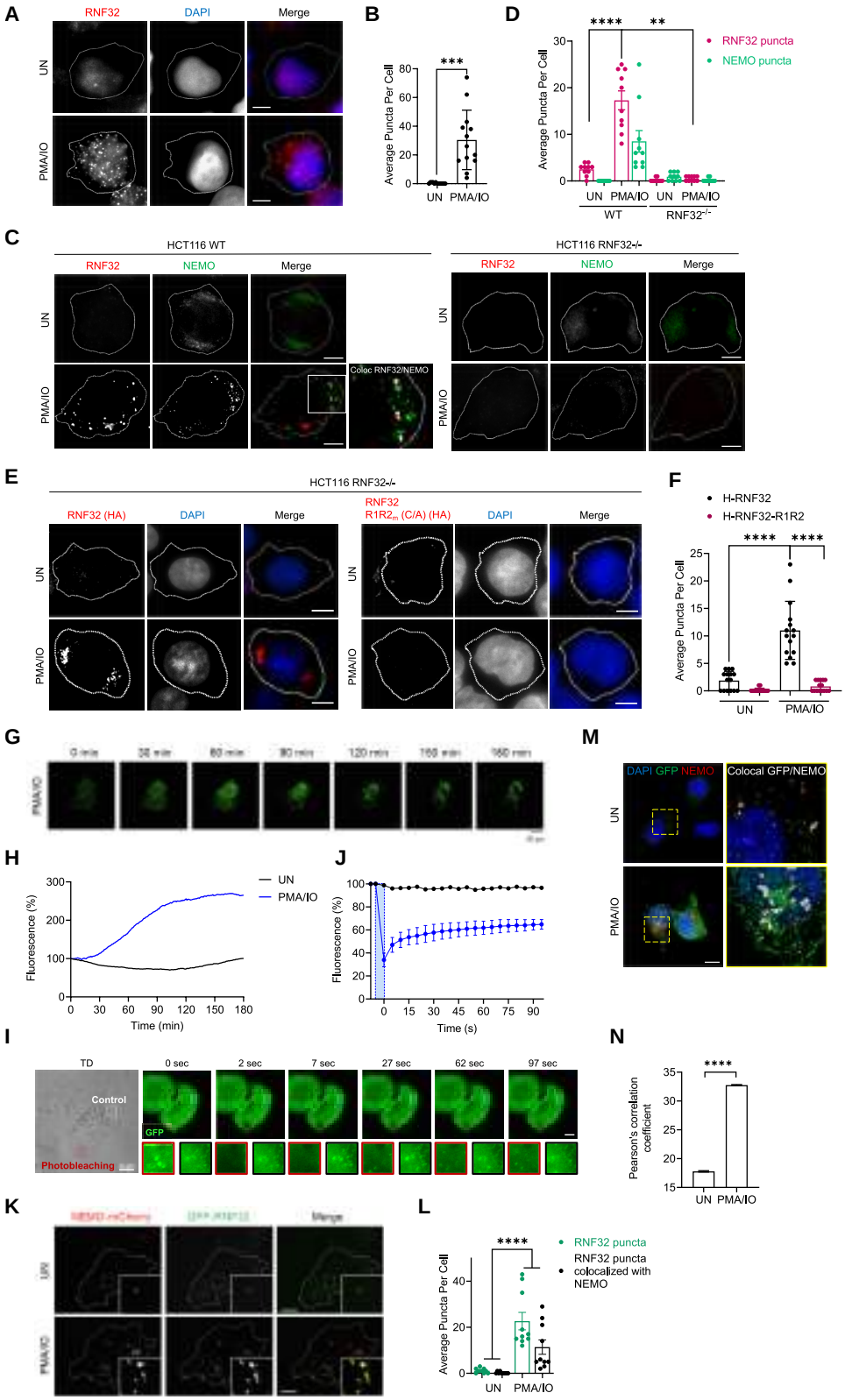

(legend on next page)

compared with RNF32 autoubiquitylation occurring in cells expressing wild-type ubiquitin. To validate these results further and test whether RNF32 is modified by Met1-linked ubiquitin chains, we performed UbiCRest analysis. RNF32 immunoprecipitated from cells treated with PMA and IO was incubated in parallel reactions with the following linkage-specific deubiquitylating enzymes previously tested to confirm their activity (Figures S6A and S6B): Lys48-specific OTUB1 (OTU deubiquitinase, ubiquitin aldehyde binding 1), Lys63-specific OTUD1 (OTU deubiquitinase 1), Met1-specific OTULIN (OTU deubiquitinase with linear linkage specificity), and the non-specific DUBs (deubiquitinating enzymes) USP2, which cleaves all linkages, and vOTU (viral OTU deubiquitinase), which cleaves all but Met1 linkages. The samples were then analyzed by immunoblotting. As shown in Figure S6C, incubation of polyubiquitylated RNF32 with Met1-specific OTULIN does not result in any detectable change either in the ubiquitin ladder (blue dashed rectangles) or in the ubiquitin moieties generated (red dashed rectangle) if compared with no DUB treatment (compare lanes 1 and 6). However, incubation of polyubiquitylated RNF32 with Lys48-specific OTUB1 or Lys63-specific OTUD1 results in both a decrease in the ubiquitin ladder and an increase in the ubiquitin moieties (mono-, di-, and tri-ub) generated. These results indicate that RNF32 is modified mainly by Lys48- and Lys63-linked ubiquitylation, although the conjugation of additional, less abundant chain types cannot be excluded. Linkage-specific anti-ubiquitin antibodies demonstrated that Lys63-linked autoubiquitylation of RNF32 is greatly induced in response to PMA/IO stimulation, whereas Lys48-linked autoubiquitylation of RNF32 is already high in untreated cells and does not increase further (Figure 4C). In agreement with UbiCRest and mass spectrometry analyses, Met1-linked ubiquitylation was not detected. Neither Lys63-linked nor Lys48-linked polyubiquitin chains were self-conjugated onto the RNF32 RING mutants (Figures 4C, 4D, and S6D). Of note, the C-terminal RING (RING 2) and the IQ CaM-binding motif are required for Lys63-linked autoubiquitylation of RNF32, whereas the N-terminal RING (RING 1) appeared to be dispensable (Figures 4D and S6D). *In vitro* ubiquitylation assays confirmed that RING2, but not RING1, is required for Lys63-linked self-ubiquitylation of RNF32 (Figure 4E).

Lys48-linked autoubiquitylation of RNF32 suggested that RNF32 is targeted for proteasomal degradation. Indeed, cycloheximide chase experiments indicate that RNF32 is a short-lived protein whose turnover is mediated by the proteasome (Figure S6E), Lys48-linked ubiquitylation (Figures S6F and S6G), and its RING domains (Figures S6H and S6I). Of note, RNF32 mutants in either RING domain were still degraded, suggesting that both RINGs contribute to RNF32 turnover (Figure S6J). The IQ CaM-binding motif appeared to be dispensable for Lys48-linked autoubiquitylation (Figure 4D) in agreement with the RNF32(I193E/Q194A) mutant being more unstable than wild-type (Figure S6K). Finally, RNF32 turnover is not strikingly affected by the stimulation with IO and PMA (Figures S6L and S6M). Taken together, these data suggest that the requirements for RNF32 proteasomal degradation are different and may not include its binding to CaM.

To further characterize the RNF32-CaM interaction and have clues on how CaM promotes RNF32 ligase activity, we employed protein structure prediction by AlphaFold2-Multimer.[18,19] The apo structure of RNF32 predicted by AlphaFold2 as in UniProt shows an extended conformation composed of several helices and including the IQ motif and the two RING domains at opposite sites (Figure 4F). Our analysis of the RNF32-CaM complex predicted with high confidence the RNF32 RINGs and IQ motif, CaM, and the relative orientation of the two proteins, as indicated by the predicted local distance difference test (pLDDT; Figure S6N) and the predicted aligned error (PAE) matrix (Figure 4G). The conformation of CaM perfectly aligned with previously solved structures of CaM-IQ domains (Figure S6O). Importantly, the binding of CaM caused a rearrangement of the RNF32 helical region between the IQ motif and RING2 (α4, α5,

Figure 3. RNF32 forms liquid-like condensates and is required for the formation of liquid phase separation of NEMO in stimulated cells

(A) Immunofluorescence staining of endogenous RNF32 in U2OS cells stimulated with PMA and ionomycin (IO) for 90 min or left untreated. Scale bars indicate 10 μm.

(B) Quantification of average numbers of RNF32 puncta per cell as shown in (A). Means ± SEM (n = 13 cells). Two-way analysis of variance (ANOVA). ***p = 0.0002.

(C) Immunofluorescence of endogenous RNF32 and NEMO in parental or RNF32$^{-/-}$ HCT116 cells stimulated as in (A). Scale bars indicate 10 μm.

(D) Quantification of average numbers of RNF32 and NEMO puncta per cell as shown in (C). Means ± SEM (n = 10 cells). Two-way ANOVA. ****p < 0.0001, **p = 0.005.

(E) RNF32$^{-/-}$ HCT116 cells re-expressing either HA-tagged WT RNF32 or the inactive RNF32(C127A/C130A/C293A/C296A) mutant (RNF32-R1R2$_m$ C/A) were stimulated as in (A). Cells were then fixed and immunostained for HA. Scale bars indicate 10 μm.

(F) Quantification of RNF32 puncta per cell as shown in (E). Means ± SEM are shown (n = 15 cells). Two-way ANOVA. ****p < 0.0001.

(G) U2OS cells expressing WT GFP-RNF32 were treated as in (A) and imaged by time-lapse microscopy for 3 hr. Scale bars represent 20 μm. n = 4 frames.

(H) Quantification of fluorescence intensity over time of the time-lapse series (n = 4) for the untreated (black line) and treated (blue line) U2OS cells as shown in (G).

(I) U2OS cells expressing WT GFP-RNF32 were treated as in (A). Live cell images showing RNF32 condensates before and after photobleaching formation are shown (red square, bleached site; white square, background). Scale bars represent 10 μm.

(J) Quantification of fluorescence intensity of the RNF32 condensates as shown in (I) over a 97-s time course in both bleached (blue line) and unbleached (black line) regions of interest. Means ± SEM (n = 10 cells).

(K) Epifluorescence images and relative magnification insets of U2OS cells expressing NEMO-mCherry and GFP-RNF32 treated as in (A). Scale bars indicate 10 μm.

(L) Quantification of puncta containing both GFP-RNF32 and mCherry-NEMO per cell as shown in (K). Means ± SEM (n = 10 cells). Two-way ANOVA. ****p < 0.0001.

(M) U2OS cells were transfected and treated as in (K). Images were acquired with a confocal laser scanning microscope. The relative magnification insets show the colocalized GFP-RNF32 and NEMO-mCherry signals (in white). Scale bars, 10 μm.

(N) Quantification of the colocalization of the two fluorophores (GFP and mCherry) as shown in (M) using Pearson's colocalization coefficient derived from 90 analyzed optical sections and expressed as percentage ± SD. n = 5 cells. ****p < 0.0001.

See also Figure S5.

CellPress
OPEN ACCESS

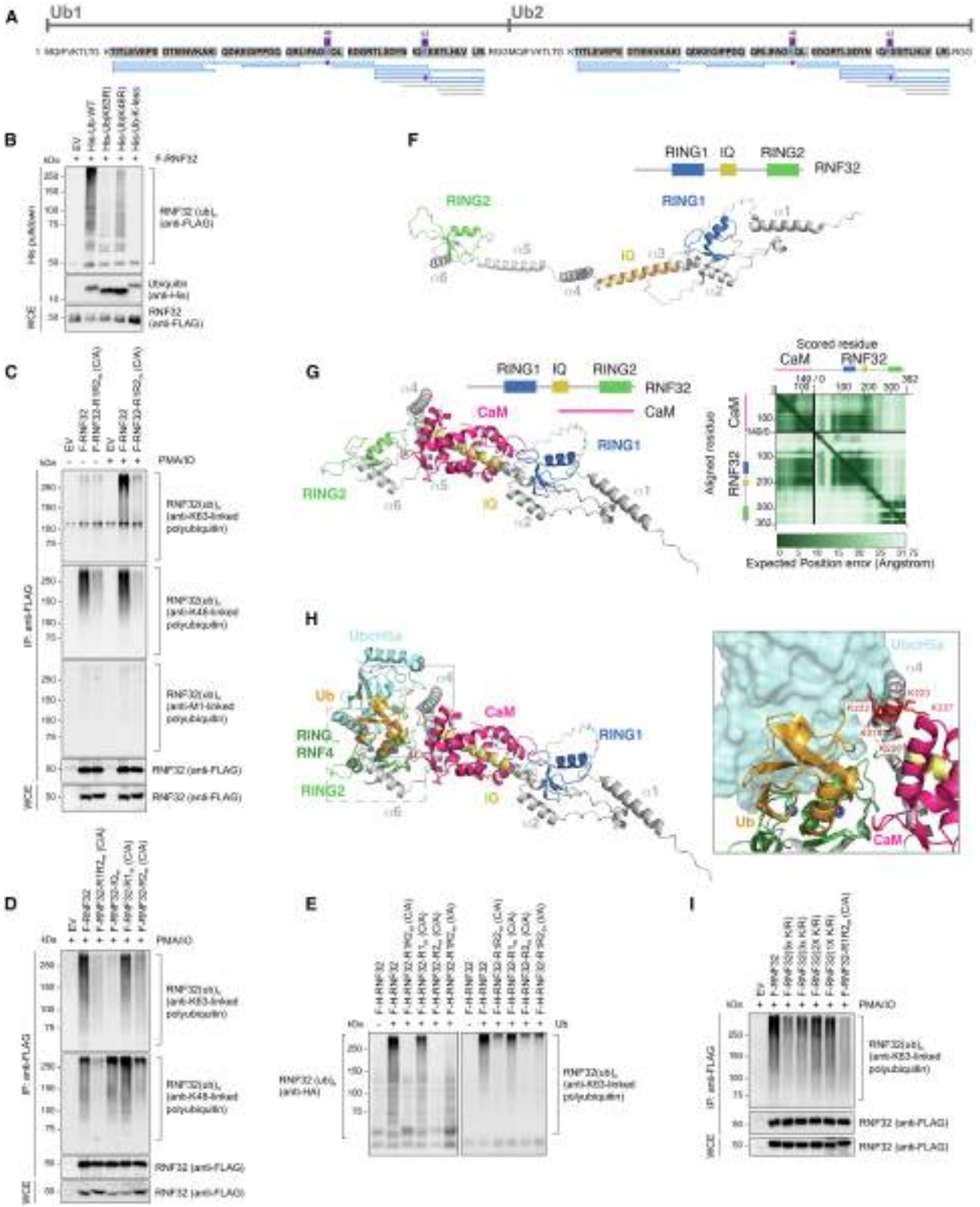

(legend on next page)

and α6 helices in Figure 4G). All predictions generated by AlphaFold2 presented this rearrangement, which is compatible with the binding of an E2 primed for catalysis, as demonstrated by the superposition of the RNF4-UbcH5A-Ub complex (Figures 4H and S6P). We noticed that in the RNF32-CaM complex, various lysine residues present in helix α4 are in close proximity to the catalytic core of the E2, perfectly positioned to perform the nucleophilic attack on the E2 catalytic site (Figure 4H). This prediction is supported by our mass spectrometry analysis, which has identified many of these lysine residues as ubiquitylated (Figure S7). To further validate these results, we generated various RNF32 mutants in which the lysine residues present in helix α4 were replaced by arginine and assessed their Lys63-linked autoubiquitylation. As shown in Figure 4I, these mutants displayed reduced Lys63-linked autoubiquitylation when compared with wild-type RNF32, with the quintuple RNF32 (K219R/K222R/K223R/K227R/K228R) mutant (RNF32[5x K/R]) displaying the least Lys63-linked autoubiquitylation, comparable with the one observed with the RNF32-R1R2$_m$ mutant.

RNF32 is required for NF-κB activation in response to bacterial LPSs

Next, we sought to identify the physiological stimuli that induce NF-κB signaling via RNF32. Increased levels of cytosolic Ca^{2+} are known to mediate NF-κB activation in response to LPSs,[20,21] which are abundant in the gut lumen. First, we confirmed that treatment of human colonic epithelial cells with LPS, but not with TNF-α or IL-1β, resulted in increased cytosolic Ca^{2+} levels (Figures 5A and 5B). Then, we tested whether RNF32 is required for activating the NF-κB signaling pathway in response to LPS. As shown in Figures 5C and 5D, LPS induced the degradation of IκBα as well as the activating phosphorylation of IKKα and IKKβ in wild-type cells but not in cells in which RNF32 expression was silenced by short interfering RNA (siRNA). The knockdown of RNF32 by siRNA also prevented the nuclear translocation of NF-κB in cells treated with LPS (Figures 5E and 5F). Likewise, RNF32 knockout SW480 cells displayed defective phosphorylation of IKKα and IKKβ in response to LPS (Figures 5G and 5H).

To investigate the role of RNF32-dependent ubiquitylation *in vivo*, we generated Rnf32 knockout mice (Figures S8A–S8C). Homozygous mutant intestines exhibited an increased number of goblet cells and fewer Paneth cells when compared with wild-type intestines, as indicated by Alcian blue and anti-lysozyme staining, respectively (Figures 6A–6D). Additionally, Rnf32$^{-/-}$ colon showed an increased number of goblet cells (Figures 6E and 6F) and augmented mucus production (Figures 6G and 6H). The number of Lgr5-positive cells was not substantially affected by Rnf32 deletion (Figure S8D), while crypt cell proliferation was slightly reduced in Rnf32-deficient guts when compared with wild-type animals (Figures S8E and S8F). Given that RNF32 is required for NF-κB activation in human cultured cells (Figures 2E–2G and 5D–5G), we examined whether Rnf32 deletion impacts NF-κB signaling in the mouse intestinal epithelium. Nuclear phospho-NF-κB-p65 staining revealed that while wild-type small intestines displayed NF-κB signaling activation primarily at the base of the crypts, this activation was markedly reduced in Rnf32-deficient small intestines (Figure 6I).

To determine whether the observed phenotype is intrinsic to intestinal epithelial cells, we utilized intestinal organoids derived from Rnf32$^{-/-}$ mice. These organoids displayed an increased number of goblet cells and fewer Paneth cells (Figures S9A–S9D), reduced NF-κB signaling (Figures S9E–S9G), and proliferation rate (Figures S9H and S9I) when compared with organoids derived from wild-type intestines. The cell fate specification defect observed in Rnf32$^{-/-}$ organoids was rescued when the NF-κB pathway was activated by knocking down the NF-κB inhibitor IκBα (Figures S9J and S9K), suggesting that the observed phenotype results from defective activation of NF-κB. In addition, treatment of intestinal organoids derived from wild-type mice with the CaM inhibitor W-7 decreased NF-κB signaling (Figure S9L).

As RNF32 expression is increased in primary colorectal tumors (Figures S2A–S2F) and is associated with decreased OS

Figure 4. Characterization of RNF32 ubiquitylation

(A) RNF32 was immunopurified and analyzed by mass spectrometry. The recovered ubiquitin peptides are shown. Ascore (= 10*LOG [*p* value] higher than 15).

(B) HEK293T cells were transfected with WT FLAG-tagged RNF32 along with His-tagged WT ubiquitin or the indicated ubiquitin mutants. Cells were lysed, and the bulk of ubiquitylated proteins was affinity-purified using nickel agarose. Purified ubiquitylated proteins were then analyzed by immunoblotting.

(C) HEK293T cells were transfected with FLAG-tagged WT RNF32 or RNF32-R1R2$_m$ (C/A) and treated with PMA and IO for 60 min or left untreated. Cells were lysed in denaturing conditions, and WCEs were immunoprecipitated with an anti-FLAG antibody. Immunoprecipitates were analyzed by immunoblotting.

(D) HEK293T cells were transfected with FLAG-tagged WT RNF32, or the indicated mutants, and treated with PMA and IO for 90 min. Cells were lysed in denaturing conditions, and WCEs were immunoprecipitated with an anti-FLAG antibody. Immunoprecipitates were then analyzed as in (C).

(E) *In vitro* ubiquitin ligation assay of immunopurified FLAG-HA-epitope-tagged RNF32 (WT or the indicated mutants) was carried out in the presence of purified recombinant E1, UBCH5B (E2), purified recombinant CaM, with or without WT ubiquitin. Samples were analyzed by immunoblotting.

(F) Ribbon diagram of the AlphaFold model of the RNF32 protein deposited on the UniProt database (AF-Q9H0A6-F1-model_v4). The structural domains of RNF32 (gray) are highlighted: the RING1 domain in blue, the IQ domain in yellow, and the RING2 domain in green.

(G) Ribbon diagram of the top-scoring AlphaFold2-Multimer model of the CaM:RNF32 interaction obtained by inputting protein sequences for the FL human CaM (residues 1–149), shown in dark pink, and FL human RNF32 (residues 1–362), shown colored as in (F). Right, the predicted aligned error (PAE) matrix for the CaM:RNF32 complex generated by AlphaFold2.

(H) Cartoon representation of the complex between CaM:RNF32 and UbcH5A-Ub in its closed conformation, primed for catalysis. RNF4-UbcH5A-Ub complex (PDB: 4AP4) was superimposed with the CaM:RNF32 complex prediction shown in (G), aligning the respective RING domains. RNF4 RING is in dark green, UbcH5a is in cyan, and Ub is in dark yellow. Other molecules are colored as in (F) and (G). Right, details of the putative interaction interface between UbcH5A-Ub and RNF32. The side chains of lysine residues on RNF32 helix α4 (aa 218–241) are depicted in red (K219-222-223-227 and 228).

(I) HEK293T cells were transfected with FLAG-tagged WT RNF32 or the indicated mutants (5x K/R: K219R/K222R/K223R/K227R/K228R; 3x K/R: K219R/K222R/K223R; 2x K/R: K227R/K228R; and 1x K/R: K219R) and treated as in (D). Cells were lysed in denaturing conditions, and WCEs were immunoprecipitated with an anti-FLAG antibody. Immunoprecipitates were analyzed by immunoblotting.

See also Figure S6.

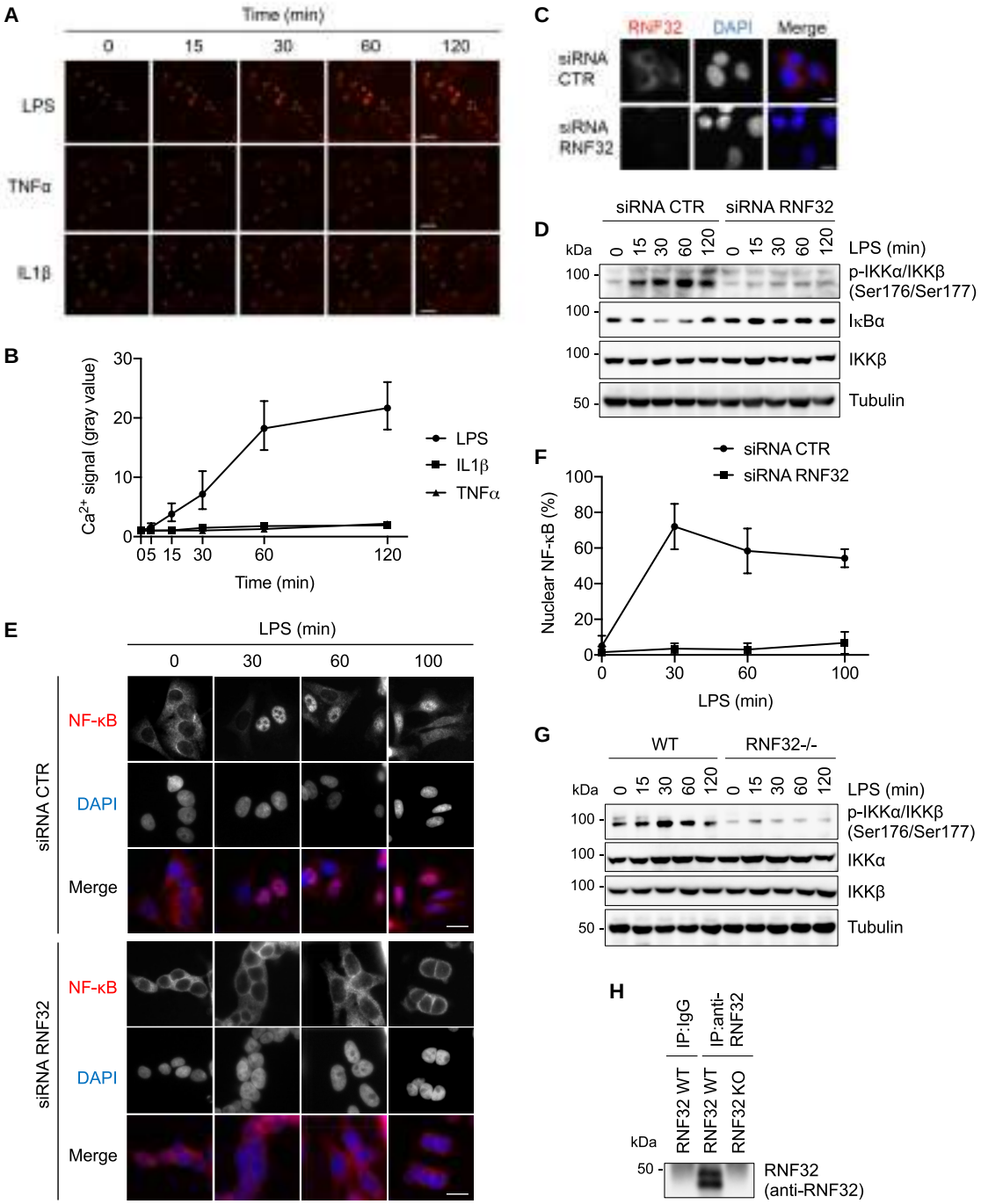

Figure 5. RNF32 is required for the NF-κB activation in response to LPSs

(A and B) SW480 cells were treated with the calcium indicator Biotracker 609 Red Ca^{2+} AM Dye and stimulated with 20 ng/ml TNF-α, 1 μg/ml IL-1β, or 10 μg/ml lipopolysaccharides (LPSs). The intensity of this fluorescent probe was measured by microscopy. Scale bar, 40 μm (A). Regions of interest (ROIs) (yellow circles) within the cells were analyzed and plotted in (B). The mean ± SEM (n = 10 cells) is shown.

(C–F) SW480 cells were transfected with the indicated siRNAs. Cells were treated with 10 μg/ml LPS and analyzed by immunofluorescence (in C to validate the knockdown of RNF32 and in (E) to assess NF-κB nuclear translocation) or lysed and processed for immunoblotting (D). Scale bar, 10 μm (C) and 20 μm (E). Quantification of the average number of cells (%) with nuclear NF-κB is shown in (F). Mean ± SEM (n = 100 cells).-

(G) Parental or RNF32ᐟ ᐟ SW480 cells were treated with LPS. Total cell extracts were analyzed by immunoblotting.

(H) Extracts from RNF32+/+ and RNF32ᐟ ᐟ SW480 cells were subjected to immunoprecipitation (IP) with an anti-RNF32 antibody, followed by immunoblotting with the same antibody.

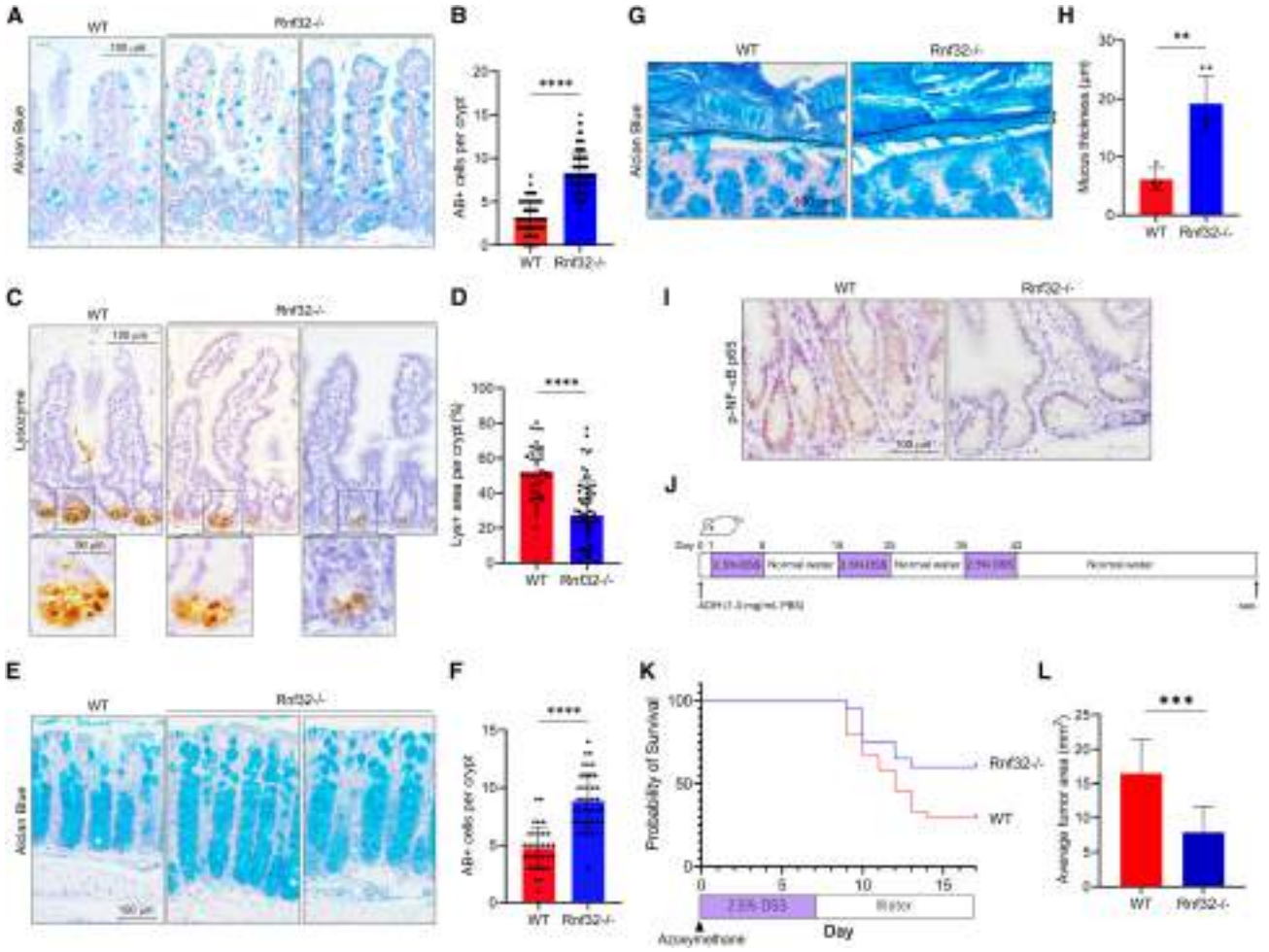

Figure 6. RNF32 controls cell fate specification

(A) Alcian blue staining on paraffin-embedded sections of the small intestine from WT and Rnf32$^{-/-}$ mice (n = 3 per group). Scale bar: 100 μm.

(B) Quantification of Alcian-blue-positive (AB^{+}) goblet cells per crypt in the small intestine. ****$p < 0.0001$ (unpaired t test). Error bars represent SEM n = 3 per group with 90 and 150 crypts analyzed per WT and Rnf32$^{-/-}$, respectively.

(C) Staining with anti-lysozyme antibody on paraffin-embedded sections of the small intestine from WT and Rnf32$^{-/-}$ mice (n = 3 per group). Scale bars: 50 and 100 μm.

(D) Quantification of the lysozyme-positive (Lys^{+}) area per crypt. The percentage of Lys^{+} area per crypt was measured using ImageJ, and the averages were calculated. ****$p < 0.0001$ (unpaired t test). Error bars represent SEM (n = 3 per group) with 37 and 66 crypts analyzed per WT and Rnf32$^{-/-}$, respectively.

(E) Alcian blue staining on paraffin-embedded sections of the colon from WT and Rnf32$^{-/-}$ mice (n = 3 per group). Scale bars: 100 μm.

(F) Quantification of AB^{+} goblet cells per upper crypt in the colon. ****$p < 0.0001$ (unpaired t test). Error bars represent SEM (n = 3 per group), with 32 and 40 crypts analyzed per WT and Rnf32$^{-/-}$, respectively.

(G) Alcian-blue-stained sections from the colon of WT and Rnf32$^{-/-}$ mice (n = 3 per group). Colonic tissues were fixed in Carnoy's fixative and stained with Alcian blue. The mucus layer indicated by dotted lines is visible. Scale bars: 100 μm.

(H) Quantification of mucus in the colon by measuring the stained area at 10 points per section using ImageJ, and the averages were calculated. ***$p < 0.001$ (unpaired t test). Error bars represent SEM n = 4 for WT and n = 6 for Rnf32$^{-/-}$.

(I) Anti-phospho-NF-κB p65 (phospho-S536) staining on paraffin-embedded sections of the small intestine of WT and Rnf32$^{-/-}$ mice (n = 3 per group). Scale bars: 100 μm.

(J) Schematic representation of the experimental timeline for the azoxymethane (AOM)/dextran sulfate sodium (DSS) model of colitis-associated colorectal cancer.

(K) Kaplan-Meier plot showing the survival probability of WT and RNF32$^{-/-}$ mice subjected to AOM/DSS, as shown in (J) (n = 12 WT mice; n = 10 KO mice).

(L) Assessment of the tumor area observed in WT and Rnf32$^{-/-}$ mice subjected to AOM/DSS. Data are mean tumor area ± SEM (n = 8 WT mice; n = 8 KO mice; *** $p < 0.005$).

See also Figures S8 and S9.

(Figure S2G), Rnf32-deficient mice were subjected to the azoxymethane (AOM)/dextran sulfate sodium (DSS) model of colitis-associated colorectal cancer (Figure 6J). As shown in Figures 6K and 6L, Rnf32 knockout mice showed higher survival rates and smaller tumors than wild-type littermates, indicating that Rnf32 depletion has a beneficial effect against colon cancer progression in the AOM/DSS-induced mouse colon cancer model and suggesting that targeting RNF32 might represent a therapeutic strategy in colorectal cancer patients.

DISCUSSION

Our study demonstrates that the uncharacterized E3 ubiquitin ligase RNF32 controls NF-κB signaling by binding and activating the IKK complex (Figure S9M). This activation mechanism is distinct from the ones induced by inflammatory cytokines such as IL-1β, which is mediated by the E3 ligase TRAF6, and TNF-α, which depends on the E3 ligases TRAF2, TRAF5, cIAP1, cIAP2, and LUBAC (linear ubiquitin chain assembly complex). Indeed, the RNF32-dependent activation of the NF-κB signaling is mediated by a rise of intracellular Ca^{2+} and its sensor protein CaM that induces the ligase activity of RNF32. This is triggered by PMA and the calcium ionophore IO, which synergize to activate NF-κB signaling bypassing surface receptor engagement, or by LPSs, outer membrane components of gram-negative bacteria that promote an increase in intracellular calcium ion concentration, leading to NF-κB activation. The identification of an E3 directly controlling the activity of the IKK complex in response to Ca^{2+} level fluctuation suggests a scenario in which different stimuli control distinct E3 ubiquitin ligases, each promoting the synthesis of poly-ubiquitin chains and liquid phase separation of NEMO, thus converging into IKK activation and subsequent activation of NF-κB.

Our data suggest that RNF32 is modified by Lys48- and Lys63-linked ubiquitin chains. It has been shown that NEMO has a higher affinity for linear Met1-linked ubiquitin when compared with Lys63-linked chains[15]; however, it has also been demonstrated that (1) in the case of long chains, full-length NEMO also binds to other ubiquitin chain types,[8] including Lys63-linked[22] and Lys11-linked[23] chains, and that (2) immobilization of NEMO, which may be reminiscent of oligomerization, facilitates the interaction with Lys63-linked ubiquitin chains.[24] In this regard, RNF32 displays both of these features: it is modified by long chains, as indicated by the high molecular weight of its self-conjugated ubiquitin chains, and forms condensates in response to an increase in intracellular calcium.

We found that RNF32 is expressed in LGR5-positive ISCs that are known to express Toll-like receptor-4 (TLR4),[25] the main receptor of LPSs. Our *in vivo* results demonstrate that RNF32 plays an essential role in the homeostasis of the intestinal epithelium. Indeed, RNF32-deficient mice have decreased Paneth cell and increased goblet cell numbers in the small intestine and a dramatic increase of goblet cells and mucus secretion in the colon. A similar phenotype was observed in Tlr4-deficient mice[26] and in a mouse model with constitutively suppressed NF-κB activity.[27] These mice, which express the IκBαΔN super-repressor that blocks NF-κB release, display an altered balance between goblet and Paneth cells in the adult small intestine.

In summary, we have identified a regulator of NF-κB signaling in the intestinal epithelium. It is well established that dysregulation of the NF-κB signaling pathway in the human gut drives various inflammatory disorders and contributes to colorectal tumorigenesis. We propose that approaches to target RNF32 could be beneficial to these conditions. Interestingly, comparing RNF32 expression in a variety of normal and tumor human samples revealed that RNF32 expression is elevated particularly in stomach, colon, and rectum adenocarcinomas, the three major gastrointestinal cancer types, and is associated with decreased OS of colon cancer patients, indicating that high RNF32 expression is an unfavorable prognostic marker in patients with colon cancer.

Limitations of the study

Although it is intriguing that RNF32 has two RING domains, our findings indicate that the N-terminal RING domain (RING1) plays a minor role in the ubiquitylation activity of RNF32. Indeed, experiments carried out in cultured cells as well as *in vitro* demonstrated that RING2, but not RING1, is required for Lys63-linked self-ubiquitylation of RNF32. The function of RING1 is currently unknown. Moreover, while we found that Lys63-linked ubiquitylation of RNF32 mediates the activation of NF-κB signaling and Lys48-linked ubiquitylation results in its proteasome-dependent degradation, it is still unclear how the balance of these two processes is regulated and whether other chain types are involved.

RESOURCE AVAILABILITY

Lead contact

Requests for further information and resources should be directed to, and will be fulfilled by, the lead contact, Daniele Guardavaccaro (daniele.guardavaccaro@univr.it).

Materials availability

Materials generated in this study are available from the lead contact upon request.

Data and code availability

- Original images have been deposited at Mendeley and are publicly available as of the date of publication. The DOI is listed in the key resources table. Proteomics data have been deposited in the ProteomeXchange Consortium via the PRIDE partner repository with the dataset identifier listed in the key resources table. RNA-seq data have been deposited in NCBI (SRA database) and are publicly available as of the date of publication. The accession number is listed in the key resources table.
- This paper does not report original code.
- Any additional information required to reanalyze the data reported in this paper is available from the lead contact upon request.

ACKNOWLEDGMENTS

The authors thank S. Kuchay, A. Peschiaroli, and O. Sangfelt for helpful comments; G. Chevreux and V. Legros for technical assistance; S. Papa for reagents; D. Ghete for providing the HT-X1 microscope; and the University of Verona Centro Piattaforme Tecnologiche for technical support. This work was funded by grants from the Fondazione Cariverona (2018.0877); the Fondazione Telethon ETS Italy (GMR22T1088); the European Union – NextGenerationEU through the Italian Ministry of University and Research under PNRR – M4C2-I1.3 project PE_00000019 "HEAL italia"; PRIN_PNRR_2022_M4C2_INV1.1_GUARDAVACCARO; the Ministry of Foreign Affairs and International Cooperation (MAECI); the Ministry of University and Research (DM737/2021) to D.G.; PRIN202223SPOLO_01 to S.P. and

D.G.; the Worldwide Cancer Research (19-0003) and the Italian Association for Cancer Research (AIRC-IG2017) to S.P.; the Fondazione Veronesi to A.L.; the Grant-in-Aid for Scientific Research (KAKENHI) from the Ministry of Education, Culture, Sports, Science, and Technology, Japan (22K19629, 22H03288, and 21KK0162); and JSPS Program for Forming Japan's Peak Research Universities:J-PEAKS (JPJS00420240022) to Y.K.

AUTHOR CONTRIBUTIONS

A.L. and J.H.E.S. conceived, planned, and carried out most experiments and co-wrote the manuscript. M.S. analyzed the RNF32 knockout mice and intestinal organoids. E.M., V.T., and S.P. performed the structural studies. M.H., F.A.R., N.V., Y.M., and M.R. carried out bioinformatic analyses. M.P. and A.A. performed biophysical characterizations. M.D. and M.A. provided purified recombinant proteins. A.Y. generated the *Rnf32*-knockout mice. S.S. oversaw data acquisition, analysis, and interpretation of live-imaging data. D.G. and Y.K. conceived, directed, and coordinated the study and co-wrote the manuscript. All authors discussed the results and read the manuscript.

DECLARATION OF INTERESTS

The authors declare no competing interests.

STAR★METHODS

Detailed methods are provided in the online version of this paper and include the following:

- KEY RESOURCES TABLE
- EXPERIMENTAL MODEL AND STUDY PARTICIPANT DETAILS
  - Cell lines
- METHOD DETAILS
  - Drug treatment
  - Histology, immunohistochemistry, and *in situ* hybridization
  - *In vitro* ubiquitylation assay
  - UbiCRest analysis
  - Plasmids
  - Transient transfection and lentivirus-mediated gene transfer
  - Identification of RNF32 interactors
  - CRISPR genome editing
  - NF-κB luciferase reporter assays
  - Biochemical methods
  - Antibodies
  - Quantitative real-time PCR
  - RNA Sequencing
  - Immunofluorescence
  - *In vitro* binding assay
  - Calmodulin production and RNF32 peptide synthesis
  - AlphaFold2-Multimer prediction
  - Time-lapse confocal imaging
  - Optical diffraction tomography
  - Fluorescence recovery after photobleaching
  - Confocal and colocalization analysis
  - Azoxymethane (AOM)/Dextran Sodium Sulfate (DSS) mouse model
  - Analysis of small intestinal organoids
  - In silico analysis of RNF32 expression in cancer
- QUANTIFICATION AND STATISTICAL ANALYSIS

SUPPLEMENTAL INFORMATION

Supplemental information can be found online at https://doi.org/10.1016/j.molcel.2025.10.005.

Received: September 11, 2024
Revised: May 6, 2025
Accepted: October 7, 2025
Published: October 29, 2025

REFERENCES

1. Beumer, J., and Clevers, H. (2021). Cell fate specification and differentiation in the adult mammalian intestine. Nat. Rev. Mol. Cell Biol. *22*, 39–53. https://doi.org/10.1038/s41580-020-0278-0.
2. Liu, X., Nagy, P., Bonfini, A., Houtz, P., Bing, X.-L., Yang, X., and Buchon, N. (2022). Microbes affect gut epithelial cell composition through immune-dependent regulation of intestinal stem cell differentiation. Cell Rep. *38*, 110572. https://doi.org/10.1016/j.celrep.2022.110572.
3. Taniguchi, K., and Karin, M. (2018). NF-κB, inflammation, immunity and cancer: coming of age. Nat. Rev. Immunol. *18*, 309–324. https://doi.org/10.1038/nri.2017.142.
4. Zhang, Q., Lenardo, M.J., and Baltimore, D. (2017). 30 Years of NF-κB: A Blossoming of Relevance to Human Pathobiology. Cell *168*, 37–57. https://doi.org/10.1016/j.cell.2016.12.012.
5. Hayden, M.S., and Ghosh, S. (2008). Shared Principles in NF-κB Signaling. Cell *132*, 344–362. https://doi.org/10.1016/j.cell.2008.01.020.
6. Chen, J., and Chen, Z.J. (2013). Regulation of NF-κB by ubiquitination. Curr. Opin. Immunol. *25*, 4–12. https://doi.org/10.1016/j.coi.2012.12.005.
7. Napetschnig, J., and Wu, H. (2013). Molecular basis of NF-κB signaling. Annu. Rev. Biophys. *42*, 443–468. https://doi.org/10.1146/annurev-biophys-083012-130338.
8. Iwai, K. (2012). Diverse ubiquitin signaling in NF-κB activation. Trends Cell Biol. *22*, 355–364. https://doi.org/10.1016/j.tcb.2012.04.001.
9. Barker, N., van Es, J.H., Kuipers, J., Kujala, P., van den Born, M., Cozijnsen, M., Haegebarth, A., Korving, J., Begthel, H., Peters, P.J., et al. (2007). Identification of stem cells in small intestine and colon by marker gene Lgr5. Nature *449*, 1003–1007. https://doi.org/10.1038/nature06196.
10. Koo, B.-K., Spit, M., Jordens, I., Low, T.Y., Stange, D.E., van de Wetering, M., van Es, J.H., Mohammed, S., Heck, A.J.R., Maurice, M.M., et al. (2012). Tumour suppressor RNF43 is a stem-cell E3 ligase that induces endocytosis of Wnt receptors. Nature *488*, 665–669. https://doi.org/10.1038/nature11308.
11. Muñoz, J., Stange, D.E., Schepers, A.G., van de Wetering, M., Koo, B.-K., Itzkovitz, S., Volckmann, R., Kung, K.S., Koster, J., Radulescu, S., et al. (2012). The Lgr5 intestinal stem cell signature: robust expression of proposed quiescent "+4" cell markers. EMBO J. *31*, 3079–3091. https://doi.org/10.1038/emboj.2012.166.
12. Deshaies, R.J., and Joazeiro, C.A.P. (2009). RING Domain E3 Ubiquitin Ligases. Annu. Rev. Biochem. *78*, 399–434. https://doi.org/10.1146/annurev.biochem.78.101807.093809.
13. Xie, X., Harrison, D.H., Schlichting, I., Sweet, R.M., Kalabokis, V.N., Szent-Györgyi, A.G., and Cohen, C. (1994). Structure of the regulatory domain of scallop myosin at 2.8 Ä resolution. Nature *368*, 306–312. https://doi.org/10.1038/368306a0.
14. Rhoads, A.R., and Friedberg, F. (1997). Sequence motifs for calmodulin recognition. FASEB J. *11*, 331–340. https://doi.org/10.1096/fasebj.11.5.9141499.
15. Rahighi, S., Ikeda, F., Kawasaki, M., Akutsu, M., Suzuki, N., Kato, R., Kensche, T., Uejima, T., Bloor, S., Komander, D., et al. (2009). Specific recognition of linear ubiquitin chains by NEMO is important for NF-kappaB activation. Cell *136*, 1098–1109. https://doi.org/10.1016/j.cell.2009.03.007.
16. Bloor, S., Ryzhakov, G., Wagner, S., Butler, P.J.G., Smith, D.L., Krumbach, R., Dikic, I., and Randow, F. (2008). Signal processing by its coil zipper domain activates IKK gamma. Proc. Natl. Acad. Sci. USA *105*, 1279–1284. https://doi.org/10.1073/pnas.0706552105.
17. Du, M., Ea, C.-K., Fang, Y., and Chen, Z.J. (2022). Liquid phase separation of NEMO induced by polyubiquitin chains activates NF-κB. Mol. Cell *82*, 2415–2426.e5. https://doi.org/10.1016/j.molcel.2022.03.037.
18. Jumper, J., Evans, R., Pritzel, A., Green, T., Figurnov, M., Ronneberger, O., Tunyasuvunakool, K., Bates, R., Žídek, A., Potapenko, A., et al. (2021).

Highly accurate protein structure prediction with AlphaFold. Nature *596*, 583–589. https://doi.org/10.1038/s41586-021-03819-2.

19. Tunyasuvunakool, K., Adler, J., Wu, Z., Green, T., Zielinski, M., Žídek, A., Bridgland, A., Cowie, A., Meyer, C., Laydon, A., et al. (2021). Highly accurate protein structure prediction for the human proteome. Nature *596*, 590–596. https://doi.org/10.1038/s41586-021-03828-1.
20. Birla, H., Xia, J., Gao, X., Zhao, H., Wang, F., Patel, S., Amponsah, A., Bekker, A., Tao, Y.-X., and Hu, H. (2022). Toll-like receptor 4 activation enhances Orai1-mediated calcium signal promoting cytokine production in spinal astrocytes. Cell Calcium *105*, 102619. https://doi.org/10.1016/j.ceca.2022.102619.
21. Wong, J.-H., Ho, K.-H., Nam, S., Hsu, W.-L., Lin, C.-H., Chang, C.-M., Wang, J.-Y., and Chang, W.-C. (2017). Store-operated Ca2+ Entry Facilitates the Lipopolysaccharide-induced Cyclooxygenase-2 Expression in Gastric Cancer Cells. Sci. Rep. *7*, 12813. https://doi.org/10.1038/s41598-017-12648-1.
22. Laplantine, E., Fontan, E., Chiaravalli, J., Lopez, T., Lakisic, G., Véron, M., Agou, F., and Israël, A. (2009). NEMO specifically recognizes K63-linked poly-ubiquitin chains through a new bipartite ubiquitin-binding domain. EMBO J. *28*, 2885–2895. https://doi.org/10.1038/emboj.2009.241.
23. Dynek, J.N., Goncharov, T., Dueber, E.C., Fedorova, A.V., Izrael-Tomasevic, A., Phu, L., Helgason, E., Fairbrother, W.J., Deshayes, K., Kirkpatrick, D.S., et al. (2010). c-IAP1 and UbcH5 promote K11-linked polyubiquitination of RIP1 in TNF signalling. EMBO J. *29*, 4198–4209. https://doi.org/10.1038/emboj.2010.300.
24. Hadian, K., Griesbach, R.A., Dornauer, S., Wanger, T.M., Nagel, D., Metlitzky, M., Beisker, W., Schmidt-Supprian, M., and Krappmann, D. (2011). NF-κB Essential Modulator (NEMO) Interaction with Linear and Lys-63 Ubiquitin Chains Contributes to NF-κB Activation. J. Biol. Chem. *286*, 26107–26117. https://doi.org/10.1074/jbc.M111.233163.
25. Neal, M.D., Sodhi, C.P., Jia, H., Dyer, M., Egan, C.E., Yazji, I., Good, M., Afrazi, A., Marino, R., Slagle, D., et al. (2012). Toll-like receptor 4 is expressed on intestinal stem cells and regulates their proliferation and apoptosis via the p53 up-regulated modulator of apoptosis. J. Biol. Chem. *287*, 37296–37308. https://doi.org/10.1074/jbc.M112.375881.
26. Sodhi, C.P., Neal, M.D., Siggers, R., Sho, S., Ma, C., Branca, M.F., Prindle, T., Russo, A.M., Afrazi, A., Good, M., et al. (2012). Intestinal Epithelial Toll-Like Receptor 4 Regulates Goblet Cell Development and Is Required for Necrotizing Enterocolitis in Mice. Gastroenterology *143*, 708–718.e5. https://doi.org/10.1053/j.gastro.2012.05.053.
27. Brischetto, C., Krieger, K., Klotz, C., Krahn, I., Kunz, S., Kolesnichenko, M., Mucka, P., Heuberger, J., Scheidereit, C., and Schmidt-Ullrich, R. (2021). NF-κB determines Paneth versus goblet cell fate decision in the small intestine. Development *148*, dev199683. https://doi.org/10.1242/dev.199683.
28. Wu, C.-J., Conze, D.B., Li, T., Srinivasula, S.M., and Ashwell, J.D. (2006). Sensing of Lys 63-linked polyubiquitination by NEMO is a key event in NF-κB activation. Nat. Cell Biol. *8*, 398–406. https://doi.org/10.1038/ncb1384.
29. Ran, F.A., Hsu, P.D., Wright, J., Agarwala, V., Scott, D.A., and Zhang, F. (2013). Genome engineering using the CRISPR-Cas9 system. Nat. Protoc. *8*, 2281–2308. https://doi.org/10.1038/nprot.2013.143.
30. Akutsu, M., Ye, Y., Virdee, S., Chin, J.W., and Komander, D. (2011). Molecular basis for ubiquitin and ISG15 cross-reactivity in viral ovarian tumor domains. Proc. Natl. Acad. Sci. USA. *108*, 2228–2233. https://doi.org/10.1073/pnas.1015287108.
31. Wang, T., Yin, L., Cooper, E.M., Lai, M.-Y., Dickey, S., Pickart, C.M., Fushman, D., Wilkinson, K.D., Cohen, R.E., and Wolberger, C. (2009). Evidence for Bidentate Substrate Binding as the Basis for the K48 Linkage Specificity of Otubain 1. J. Mol. Biol. *386*, 1011–1023. https://doi.org/10.1016/j.jmb.2008.12.085.
32. Mevissen, T.E.T., Hospenthal, M.K., Geurink, P.P., Elliott, P.R., Akutsu, M., Arnaudo, N., Ekkebus, R., Kulathu, Y., Wauer, T., El Oualid, F., et al. (2013). OTU Deubiquitinases Reveal Mechanisms of Linkage Specificity and Enable Ubiquitin Chain Restriction Analysis. Cell *154*, 169–184. https://doi.org/10.1016/j.cell.2013.05.046.
33. Keusekotten, K., Elliott, P.R., Glockner, L., Fiil, B.K., Damgaard, R.B., Kulathu, Y., Wauer, T., Hospenthal, M.K., Gyrd-Hansen, M., Krappmann, D., et al. (2013). OTULIN Antagonizes LUBAC Signaling by Specifically Hydrolyzing Met1-Linked Polyubiquitin. Cell *153*, 1312–1326. https://doi.org/10.1016/j.cell.2013.05.014.
34. Miyoshi, H., and Stappenbeck, T.S. (2013). In vitro expansion and genetic modification of gastrointestinal stem cells in spheroid culture. Nat. Protoc. *8*, 2471–2482. https://doi.org/10.1038/nprot.2013.153.
35. Yuniati, L., Lauriola, A., Gerritsen, M., Abreu, S., Ni, E., Tesoriero, C., Onireti, J.O., Low, T.Y., Heck, A.J.R., Vettori, A., et al. (2020). Ubiquitylation of the ER-Shaping Protein Lunapark via the CRL3KLHL12 Ubiquitin Ligase Complex. Cell Rep. *31*, 107664. https://doi.org/10.1016/j.celrep.2020.107664.
36. Enriqué Steinberg, J.H., Rossi, F.A., Magliozzi, R., Yuniati, L., Santucci, M., Rossi, M., Guardavaccaro, D., and Lauriola, A. (2023). SCFβTrCP-mediated degradation of SHARP1 in triple-negative breast cancer. Cell Death Dis. *14*, 726. https://doi.org/10.1038/s41419-023-06253-6.
37. Magliozzi, R., Low, T.Y., Weijts, B.G.M.W., Cheng, T., Spanjaard, E., Mohammed, S., van Veen, A., Ovaa, H., de Rooij, J., Zwartkruis, F.J.T., et al. (2013). Control of epithelial cell migration and invasion by the IKKβ- and CK1α-mediated degradation of RAPGEF2. Dev. Cell *27*, 574–585. https://doi.org/10.1016/j.devcel.2013.10.023.
38. Pedretti, M., Favretto, F., Troilo, F., Giovannoni, M., Conter, C., Mattei, B., Dominici, P., Travaglini-Allocatelli, C., Di Matteo, A., and Astegno, A. (2023). Role of myristoylation in modulating PCaP1 interaction with calmodulin. Plant Physiol. Biochem. *203*, 108003. https://doi.org/10.1016/j.plaphy.2023.108003.
39. Astegno, A., La Verde, V., Marino, V., Dell'Orco, D., and Dominici, P. (2016). Biochemical and biophysical characterization of a plant calmodulin: Role of the N- and C-lobes in calcium binding, conformational change, and target interaction. Biochim. Biophys. Acta *1864*, 297–307. https://doi.org/10.1016/j.bbapap.2015.12.003.
40. La Verde, V., Trande, M., D'Onofrio, M., Dominici, P., and Astegno, A. (2018). Binding of calcium and target peptide to calmodulin-like protein CML19, the centrin 2 of Arabidopsis thaliana. Int. J. Biol. Macromol. *108*, 1289–1299. https://doi.org/10.1016/j.ijbiomac.2017.11.044.
41. Ewels, P.A., Peltzer, A., Fillinger, S., Patel, H., Alneberg, J., Wilm, A., Garcia, M.U., Di Tommaso, P., and Nahnsen, S. (2020). The nf-core framework for community-curated bioinformatics pipelines. Nat. Biotechnol. *38*, 276–278. https://doi.org/10.1038/s41587-020-0439-x.
42. Sgarzi, M., Mazzeschi, M., Santi, S., Montacci, E., Panciera, T., Ferlizza, E., Girone, C., Morselli, A., Gelfo, V., Kuhre, R.S., et al. (2023). Aberrant MET activation impairs perinuclear actin cap organization with YAP1 cytosolic relocation. Commun. Biol. *6*, 1044. https://doi.org/10.1038/s42003-023-05411-y.
43. Riccio, M., Dembic, M., Cinti, C., and Santi, S. (2004). Multifluorescence labeling and colocalization analyses. Methods Mol. Biol. *285*, 171–177. https://doi.org/10.1385/1-59259-822-6:171.
44. Cavallo, C., Merli, G., Zini, N., D'Adamo, S., Cattini, L., Guescini, M., Grigolo, B., Di Martino, A., Santi, S., Borzì, R.M., et al. (2022). Small Extracellular Vesicles from Inflamed Adipose Derived Stromal Cells Enhance the NF-κB-Dependent Inflammatory/Catabolic Environment of Osteoarthritis. Stem Cells Int. *2022*, 9376338. https://doi.org/10.1155/2022/9376338.
45. Sun, W., Gao, J., Yang, B., Chen, X., Kang, N., and Liu, W. (2023). Protocol for colitis-associated colorectal cancer murine model induced by AOM and DSS. Star Protoc. *4*, 102105. https://doi.org/10.1016/j.xpro.2023.102105.

STAR★METHODS

KEY RESOURCES TABLE

REAGENT or RESOURCE	SOURCE	IDENTIFIER
Antibodies		
Rabbit polyclonal anti-RNF32	Merck	Cat# HPA073560; RRID: AB_2686616
Mouse polyclonal anti-RNF32	Abnova	Cat# H00140545-B02P; RRID: AB_1018683
Rabbit polyclonal anti-FLAG	Merck	Cat# F7425; RRID: AB_439687
Mouse monoclonal anti-FLAG	Merck	Cat# F3165; RRID: AB_259529
Mouse monoclonal anti-HA	Biolegend	Cat# 901514; RRID: AB_2565336
Rabbit monoclonal anti-HA	Cell Signaling Technology	Cat# 3724; RRID: AB_1549585
Mouse monoclonal anti-β-actin	Santa Cruz Biotechnology	Cat# sc-69879; RRID: AB_1119529
Mouse monoclonal anti-MYC	Merck	Cat# M5546; RRID: AB_260581
Mouse monoclonal Ubiquitin (P4D1) (HRP Conjugate)	Cell Signaling Technology	Cat# 14049; RRID: AB_2798376
Rabbit monoclonal anti-Ubiquitin Lys63-linkage-specific	Merck	Cat# 05-1308; RRID: AB_1587580
Rabbit monoclonal anti-Ubiquitin Lys48-linkage-specific	Merck	Cat# ZRB2150; RRID: AB_2928997
Rabbit monoclonal anti-Linear Ubiquitin	Merck	Cat# ZRB2114; RRID: AB_2938573
Rabbit monoclonal anti-Ubiquitin K48-linkage-specific	Cell Signaling Technology	Cat# 8081; RRID: AB_10859893
Rabbit monoclonal anti-Calmodulin	Abclonal	Cat# A4885; RRID: AB_2863373
Mouse monoclonal anti-His	Aviva Systems Biology	Cat# OAEA00010; RRID: AB_10874637
Rabbit monoclonal anti-p-IKKα (Ser176)/p-IKKβ (Ser177)	Cell Signaling Technology	Cat# 2078; RRID: AB_2079379
Rabbit monoclonal anti-p-IKKα (Ser176)/p-IKKβ (Ser180)	Cell Signaling Technology	Cat# 2697; RRID: AB_2079382
Rabbit polyclonal anti-Myc	Cell Signaling Technology	Cat# 2272; RRID: AB_10692100
Mouse monoclonal anti-Tubulin	Calbiochem	Cat# CP06; RRID: AB_2617116
Rabbit polyclonal anti-NEMO/IKKγ	Cell Signaling Technology	Cat# 2685; RRID: AB_2124829
Mouse monoclonal anti-NEMO/IKKγ	BD Biosciences	Cat# 611306; RRID: AB_398832
Rabbit polyclonal anti-IKKα	Santa Cruz Biotechnology	Cat# sc-7184; RRID: AB_649197
Rabbit monoclonal anti-IKKβ	Cell Signaling Technology	Cat# 8943; RRID: AB_11024092
Mouse monoclonal anti-p-IκBα (Ser32/36)	Cell Signaling Technology	Cat# 9246; RRID: AB_2267145
Mouse monoclonal anti-IkBα	Cell Signaling Technology	Cat# 4814; RRID: AB_390781
Rabbit monoclonal anti-NF-κB p65	Cell Signaling Technology	Cat# 4764; RRID: AB_823578
Mouse monoclonal anti-p27	BD Biosciences	Cat# 610242; RRID: AB_397637
Rabbit monoclonal anti-p21	Cell Signaling Technology	Cat# 2947; RRID: AB_823586
Rabbit monoclonal anti-Lysozyme	Abcam	Cat# ab108508; RRID: AB_10861277
Rabbit polyclonal anti-Ki-67	Abcam	Cat# ab15580; RRID: AB_443209
Rabbit polyclonal anti-NF-κB p65 (phospho-S536)	Abcam	Cat# ab86299; RRID: AB_1925243
Rabbit polyclonal anti-NF-κB p65	Abcam	Cat# ab16502; RRID: AB_443394
Mouse IgG, HRP-linked whole Ab (from sheep)	Cytiva	Cat# NA931; RRID: AB_772210
Rabbit IgG, HRP-linked whole Ab (from donkey)	Cytiva	Cat# NA934; RRID: AB_772206
Donkey anti-Rabbit IgG Secondary Antibody, Alexa Fluor™ 488	Thermo Fisher Scientific	Cat# A21206; RRID: AB_2535792
Goat anti-Mouse IgG Secondary Antibody, Alexa Fluor™ 488	Thermo Fisher Scientific	Cat# A11029; RRID: AB_2534088
Goat anti-Mouse IgG Secondary Antibody, Alexa Fluor 594	Thermo Fisher Scientific	Cat# A11005; RRID: AB_2534073
Donkey anti-Rabbit IgG Secondary Antibody, Alexa Fluor™ 568	Thermo Fisher Scientific	Cat# A10042; RRID: AB_2534017

(*Continued on next page*)

Continued

REAGENT or RESOURCE	SOURCE	IDENTIFIER
Biological samples		
A-FLX™ Animal Tissue FFPE BALB/C Mouse Multi Tissue	Acepix Biosciences	Cat# 7010-8020
Chemicals, Peptides, and Recombinant Proteins		
Alcian blue solution, pH2.5	Wako	Cat# 015-13805
Proteasome Inhibitor MG132	PeptaNova GmbH	Cat# 3175-V
Lipofectamine RNAiMAX	Thermo Fisher Scientific	Cat# 13778100
TransIT-X2 transfection reagent	Mirus Bio MIR	Cat# 6003
Polyethylenimine	Polysciences	Cat# 23966
Polybrene	Merck	Cat# H9268
Puromycin dihydrochloride	Merck	Cat# 540411
Poly-L-lysine	Merck	Cat# P4707
MLN-4924	Selleck Chemical	Cat# S7109
Cycloheximide	Merck	Cat# C4859
Thapsigargin	Tocris	Cat# 1138
Ionomycin	Merck	Cat# I0634
Phorbol 12-myristate 13-acetate	Merck	Cat# P8139
TNFα	Peprotech	Cat# 200-01B
LPS	Thermo Fisher Scientific	Cat# 00-4976-93
W-7 hydrochloride	MedChemExpress	Cat# HY-100912
Calmidazolium	MedChemExpress	Cat# HY-103319
BioTracker 609 Red Ca2+ AM Dye	Merck	Cat# SCT021
FLAG peptide	Merck	Cat# 4799
RNF32 peptide	GenScript Inc.	N/A
Calmodulin-Sepharose 4B beads	Cytiva	Cat# 17052901
Ubiquitin-K0 human	Merck	Cat# SRP6174
Ubiquitin-K0 human	R&D Systems products	Cat# UM-NOK
Ubiquitin, Methylated, Human	Merck	Cat# 662065
Y-27632	Wako	Cat# 030-24021
SB431542	Wako	Cat# 192-16541
EDTA 2Na	Nacalai Tesque Inc.	Cat# 15130-95
BSA	SIGMA	Cat# A4503-50G
Azoxymethane	MP Biomedicals	Cat# 183971
Dextran sulfate sodium	MP Biomedicals	Cat# 160110
Critical Commercial Assays		
QuickChange Site-Directed Mutagenesis Kit	Stratagene	Cat# 200518
Dual-Luciferase Reporter Assay System	Promega	Cat# E1910
RNAscope™ Assay	ACDBio	N/A
RNAscope® Hydrogen Peroxide solution	ACDBio	Cat# 322335
1X RNAscope® Target retrieval solution	ACDBio	Cat# 322000
RNAscope® Protease Plus	ACDBio	Cat# 322331
RNAscope® Probe RNF32	ACDBio	Cat# 890381
RNAscope® Probe Lgr5	ACDBio	Cat# 312171
RNAscope® probe DapB	ACDBio	Cat# 310043
RNAscope® 2.5 HD assay-BROWN kit	ACDBio	Cat# 322310
RNAscope® 2.5 HD assay-RED kit	ACDBio	Cat# 322350
Histofine® SAB-PO (M) kit	Nichirei Biosciences Inc.	Cat# 414314
Histofine® DAB Substrate kit	Nichirei Biosciences Inc.	Cat# 425011
TNT Quick Coupled Transcription/Translation System	Promega	Cat# L1170

(*Continued on next page*)

Continued

REAGENT or RESOURCE	SOURCE	IDENTIFIER
GeneArt™ Site-Directed Mutagenesis System	Thermo Fisher Scientific	Cat# A13282
RNeasy plus Mini kit	Qiagen	Cat# 74134
SuperScript™ II Reverse Transcriptase	Thermo Fisher Scientific	Cat# 18064014
GoTaq® qPCR Master Mix	Promega	Cat# A6001
Deposited data		
Raw mass spectrometry proteomics data	ProteomeXchange	PRIDE: PXD066536
Raw RNA-seq data	NCBI	SRA: PRJNA1295885
Unprocessed and uncompressed data	This paper, Mendeley data	Mendeley Data: https://doi.org/10.17632/t2bdkr74s7.1
Experimental Models: Cell Lines		
Human U2OS	ATCC	Cat# HTB-96; RRID: CVCL_0042
Human HEK293T	ATCC	Cat# CRL-11268; RRID: CVCL_1926
Human HCT116	ATCC	Cat# CCL-247; RRID: CVCL_0291
Human SW480	ATCC	Cat# CCL-228; RRID: CVCL_0546
L-WRN	ATCC	Cat# CRL-3276; RRID: CVCL_DA06
Experimental models: Organisms/strains		
C57BL/6J Rnf32-/- mice	This paper	N/A
Oligonucleotides		
ON-TARGETplus SMARTpool RNF32 siRNA oligonucleotides	Dharmacon	Cat# L-007136-00-0005
Recombinant DNA		
pCMV3-C-FLAG-RNF32	Sino Biological	Cat# HG24274-UT
pET-21a-hCaM	GenScript	N/A
pcDNA3.1-hCaM-TEV-MYC-HIS	This paper	N/A
pcDNA3.1-FLAG-FLAG-HA-HA-RNF32 WT and mutants	This paper	N/A
pcDNA3.1-HA-RNF32	This paper	N/A
pEGFP-RNF32	This paper	N/A
pCMV-TAG-NEMO	Wu et al.[28]	Addgene Cat# 11970
pmCherry-NEMO	This paper	N/A
pEF4-FLAG-IKKα	Provided by V. D'Angiolella	N/A
pEF4-FLAG-IKKβ	Provided by V. D'Angiolella	N/A
pNf-κB-luc	Provided by S. Papa	N/A
pRL-TK	Provided by S. Papa	N/A
pcDNA3.1-His-Ubiquitin-WT	This paper	N/A
pcDNA3.1-His-Ubiquitin-K/R mutants	This paper	N/A
pWC7-His-MYC-Ubiquitin WT and mutants	This paper	N/A
pcDNA3.1-FLAG-Ubiquitin-K63-only	This paper	N/A
pHAGE2-EF1α-IRES-puromycin-RNF32 WT and mutants	This paper	N/A
pcDNA3.1-FLAG-STREP-RNF32	This paper	N/A
pET-3a-Ubiquitin	This paper	N/A
pET21-His-UBA1	This paper	N/A
pET15-His-UbE2D2	This paper	N/A
pSpCas9(BB)-2A-GFP (PX458)	Ran et al.[29]	Addgene Cat# 48138
pGEX-USP2 (aa 259-605)	This paper	N/A
pOPINK-vOTU (aa 1-183)	Akutsu et al.[30]	Addgene Cat# 61589
pProEx-hOTUB1	Wang et al.[31]	Addgene Cat# 26959

(*Continued on next page*)

Continued

REAGENT or RESOURCE	SOURCE	IDENTIFIER
pOPINK-OTUD1 (OTU+UIM, aa 287-481)	Mevissen et al.[32]	Addgene Cat# 61406
pOPINB-OTULIN (full-length, aa 1-352)	Keusekotten et al.[33]	Addgene Cat# 61464
Software and Algorithms		
ImageJ	NIH	https://imagej.nih.gov/ij/
AlphaFold2-Multimer prediction	nf-core pipeline: proteinfold 1.1.0dev (revision c246c853c6)	https://nf-co.re/
PyMOL v2.5.0	Schrodinger, LLC	http://www.pymol.org
GraphPad Prism	GraphPad Software	https://www.graphpad.com/features
Benchling CRISPR Genome Engineering tool	Benchling	https://www.benchling.com/crispr
TomoStudioTM software version X 1.6	Tomocube Inc., Korea	N/A
Richardson-Lucy deconvolution algorithm using NIS-Elements Advanced Research software	Nikon	N/A
NIS-Elements HC software version 5.20	Nikon	N/A
Other		
Advanced DMEM/F12	Gibco	Cat# 12634010
GlutaMAX™ Supplement	Gibco	Cat# 35050061
Penicillin-Streptomycin Solution (×100)	Wako	Cat# 168-23191
Intesticult™ organoid growth medium (mouse)	STEMCELL Technologies	Cat# ST-06005
Matrigel Matrix Basement Membrane Growth factor reduced Phenol red free	Corning	Cat# 356231
Fetal Bovine serum	Nichirei Biosciences Inc.	Cat# 175012
TrypLE™ Express Enzyme (1X), no phenol red	Gibco	Cat# 12604013

EXPERIMENTAL MODEL AND STUDY PARTICIPANT DETAILS

Cell lines

HCT116, HEK293T, SW480, and U2OS cells were maintained in Dulbecco's modified Eagle's medium (DMEM; Thermo Fisher Scientific 31966021) containing 10% fetal calf serum (Merck F7524), 100 μg/ml streptomycin, and 100 U/ml penicillin (Thermo Fisher Scientific 15070063). All cell lines were maintained at 37°C and 5% CO_2 in a humidified atmosphere.

Animal procedures

All animal work was performed in accordance with the ethical guidelines and protocols approved by the Committee on Animal Experiments of Tokushima University (#T-2022-23). Deletion of Rnf32 in mouse zygotes was achieved by electroporating a Cas9-gRNA ribonucleoprotein complex (RNP) mixture, composed of two crRNAs targeting intron 2 and intron 6 of Rnf32. Briefly, two crRNAs were first hybridized with tracrRNA and then assembled with recombinant Cas9 protein, using the Alt-R CRISPR-Cas9 System (IDT). One-cell zygotes were prepared by in vitro fertilization of C57BL/6J mouse oocytes and sperm. Electroporation was performed using a Genome Editor electroporator (BEX Co) and an LF501PT1-5 platinum plate electrode (BEX Co). Thirty to forty zygotes were aligned in the electrode gap filled with 5 μl of Opti-MEM I containing the RNP complex and subjected to electroporation at 20V (3 msec ON + 97 msec OFF) for seven cycles. After an overnight culture, the resulting two-cell embryos were transferred into the oviducts of pseudo-pregnant MCH/ICR females. Heterozygous mice expressing deleted Rnf32 were crossed to generate Rnf32-/- mice. Deletion of target sites was confirmed by PCR and sequencing. The following primers were used for genotyping: Rnf32 int2 Fw, 5'-TTATGCAGAACAGTCCCTTGGAA-3'; int2 Rv, 5'-CTGTTTGTGTTTTGGCAAGAAGG-3'; int5 Fw, 5'-GGTTTTGT GGTATTGGGGTCATT-3'; int6 Rv, 5'-CAGCTTTGATGTGCAGGTAACAA-3'. Expression of Rnf32 in intestinal tissues was examined by RT-PCR using the following primers: Fw, 5'-TCGGATGCCAAATTAAGGAG-3'; Rv, 5-ATCTGGCCACACCTTTCATC-3'.

Rnf32-/- mice and their littermate controls (C57BL/6J background), all males of 8–12 weeks of age, were used for the Azoxymethane (AOM)/Dextran Sodium Sulfate (DSS) model.

Establishment and maintenance of small intestinal organoids

Murine intestinal crypt cells were isolated from proximal small intestines by incubation for 30 minutes at 4°C in PBS containing 2 mM EDTA. The isolated crypts were then mixed with 50% growth factor-reduced, phenol-red-free Matrigel (#356231, Corning) diluted with Advanced DMEM/F12 and plated in 24-well plates. After polymerization, 500 μL of complete organoid culture medium (50% L-WRN conditioned medium) was used for culturing organoids.[34]

METHOD DETAILS

Drug treatment

Where indicated, cells were treated with 10 μM MG132 (PeptaNova GmbH 3175-v), 0.5 μM MLN4924 (Selleck Chemical S7109), 100 μM cycloheximide (Merck C4859), 100 nM thapsigargin (Tocris 1138), 950 nM ionomycin (IO) (Merck I0634), 10 ng/ml phorbol 12-myristate 13-acetate (PMA) (Merck P8139), 20 ng/ml TNFα (Peprotech 300ｰ 01Ａ), 1 μg/ml IL-1β (PeproTech 200-01B), 10 μg/ml LPS (Thermo Fisher Scientific 00-4976-93), 25, 50 or 100 μM W-7 hydrochloride (MedChemExpress), 10 μM calmidazolium (MedChemExpress). HCT116 and SW480 cells were stained with BioTracker 609 Red Ca^{2+} AM Dye according to the manufacturer's instructions (Merck SCT021).

Histology, immunohistochemistry, and *in situ* hybridization

Histological analysis was performed on intestinal sections from 8–12-week-old sex-matched littermate mice. Tissues were fixed in 4% paraformaldehyde overnight at room temperature, followed by dehydration and paraffin embedding. Five-μm paraffin-embedded intestinal sections were deparaffinized and rehydrated. Alcian blue (AB)-stained sections were prepared to assess the number of Goblet cells. Briefly, 3% acetic acid was applied to the slides for 3 minutes, followed by the addition of AB solution (#4987481211568, FUJIFILM) for 30 minutes. The slides were then rinsed in running tap water and dehydrated with an ascending ethanol gradient (70%, 95%, and 100%). Slides were mounted, and images were acquired under bright field using an Olympus BX53 light microscope (Olympus, Japan).

For mucus staining, mouse colorectal tissues were fixed in Carnoy's fixative at 4°C overnight to preserve the mucus layer and then processed for paraffin embedding. Four-μm-thick sections were cut with a microtome and stained with AB solution. Measurements were taken at 10 positions per section using ImageJ, and the averages were calculated.

For immunohistochemical (IHC) analysis, paraffin-embedded intestinal sections were deparaffinized and subjected to heat-induced antigen retrieval in 10 mM citrate buffer (pH 6.0). Sections were incubated with primary antibodies and stained using a Histofine® SAB-PO (M) kit (Nichirei, Japan), followed by counterstaining with hematoxylin.

In situ hybridization (ISH) was performed using a commercially available kit according to the manufacturer s recommendations (ACDBio). All procedures, including deparaffinization, hydration, and antigen retrieval, were conducted to minimize RNase contamination. Paraffin-embedded sections along with tissue controls were baked, deparaffinized, and incubated with RNAscope® Hydrogen Peroxide solution (#322335) for 10 minutes at room temperature. Antigen retrieval was carried out in 1X RNAscope® Target retrieval solution (#322000) for 15 minutes at 100°C, followed by protease digestion with RNAscope® Protease Plus (#322331) for 15 minutes at 40°C. Probes were then hybridized with RNAscope® Probe RNF32 (#890381) or Lgr5 (#312171) for 2 hours at 40°C. The signals were amplified and detected with RNAscope® 2.5 HD assay-BROWN kit (#322310) or RNAscope® 2.5 HD assay-RED kit (#322350). The RNAscope® probe DapB (#310043) was used as a negative control. Each single RNA transcript appeared as a distinct dot of brown chromogen precipitate visible under bright field using an Olympus BX53 light microscope.

In vitro ubiquitylation assay

In vitro ubiquitylation of RNF32 was performed in a volume of 20 μl containing 50 mM Tris pH 7.6, 2 mM $CaCl_2$, 5 mM $MgCl_2$, 5 mM ATP, 1 μM purified recombinant E1, 10 μM UBCH5B, immunopurified RNF32 (WT or mutants) in the presence or absence of 0.5 μg/μl purified recombinant CaM, 300 μM wild-type ubiquitin, 300 μM Lys-less ubiquitin, or 300 μM methylated ubiquitin. Reactions were incubated at 30°C for 30-40 minutes and analyzed by immunoblotting.

UbiCRest analysis

HEK293T cells were transfected with pcDNA3.1-FLAG-HA-RNF32 and treated with PMA and ionomycin for 90 minutes. Cells were harvested and lysed in IP lysis buffer (50 mM Tris pH 7.5, 250 mM NaCl, 1% Triton X-100, 1 mM EDTA, 50 mM NaF, 5 mM N-ethylmaleimide and protease and phosphatase inhibitors). RNF32 was immunopurified with anti-FLAG agarose resin (Merck A2220). Beads were washed with IP lysis buffer 4 times and once in 1 mL of 1X DUB Reaction Buffer (50 mM Tris pH 7.5, 50 mM NaCl, 5 mM DTT). Beads were resuspended in DUB dilution buffer (25 mM Tris pH 7.5, 150 mM NaCl, 10 mM DTT) and transferred into separate tubes for subsequent DUB incubations. To perform UbiCRest, 5X concentrated DUB stocks were prepared on ice by diluting enzymes using DUB dilution buffer, and were preincubated at room temperature for 10-15 min. DUBs were used at the following final concentrations: 1.5 μM USP2, 0.5 μM vOTU, 20 μM OTUB1, 1 μM OTUD1, and 5 μM OTULIN. The samples were placed on a dry heat block at 37°C. After 120 min, the reaction was stopped by adding 5X Laemmli sample buffer.

Plasmids

Human RNF32 and Calmodulin cDNAs were obtained from Sino Biological and GenScript, respectively. RNF32 carrying N-terminal 2xFLAG-2xHA or single HA were subcloned into pcDNA3. Wild-type RNF32 was also subcloned into pEGFP-C1. pCMV-TAG-NEMO (Addgene 11970) was a gift from Jon Ashwell. Wild-type NEMO was subcloned in pmCherry-N1. FLAG-tagged IKKα and IKKβ were gifts from Vincenzo D'Angiolella. pNf-κB-luc and pRL-TK were gifts from Salvatore Papa. His-tagged wild-type ubiquitin and K/R mutants were subcloned into pcDNA3.1. All mutants were generated using the GeneArt™ Site-Directed Mutagenesis System (Thermo Fisher Scientific A13282) according to the manufacturer's instructions.

Transient transfection and lentivirus-mediated gene transfer

For gene silencing, ON-TARGETplus SMARTpool RNF32 siRNA oligonucleotides (Dharmacon L-007136-00-0005) were transfected into cells using RNAiMax (Thermo Fisher Scientific 13778100) according to the manufacturer's instructions (two rounds of transfections were performed). Plasmids were transiently transfected using TransIT-X2 Transfection reagent (Mirus Bio MIR 6003) except for HEK293T and U2OS cells which were transfected using the polyethylenimine (PEI) (Polysciences 23966).

For lentiviral transduction, wild-type RNF32 and mutants were subcloned into pHAGE2-EF1α-IRES-puromycin vectors. HEK293T cells were transfected by the PEI method with the pHAGE2 vectors together with packaging vectors (Gag-Pol, Rev, Tat, and the G protein of the vesicular stomatitis virus). Supernatants were collected 24 hours after transfection, filtered, and transferred to cells with 4 μg/ml polybrene (Merck H9268). Cells were selected with 1 ug/ml puromycin dihydrochloride (Merck 540411).

Identification of RNF32 interactors

RNF32 interactors were identified as described.[35–37] Briefly, HEK293T cells were transfected with pcDNA3-FLAG-HA-RNF32 and treated with 10 μM MG132 for 5 hr. Cells were harvested and lysed in lysis buffer (50 mM Tris-HCl pH 7.5, 150 mM NaCl, 1 mM EDTA, 1 mM $MgCl_2$, 10% glycerol and 0.5% NP-40 plus protease and phosphatase inhibitors). RNF32 was immunopurified with anti-FLAG agarose resin (Merck A2220). Beads were washed, and proteins were eluted by competition with FLAG peptide (Merck 4799). The eluate was then subjected to a second immunopurification with anti-HA resin (Roche 11815016001). Beads were washed, and proteins were eluted using RapiGest SF (Waters 186001861). The eluate was subsequently treated with reduction buffer (1 μg/μl dithiothreitol) for 30 minutes and alkylation buffer (5 μg/μl iodoacetamide) for 20 minutes, followed by Lys-C for 4 hours. Trypsin was added at a 1:50 ratio, and the mixture was incubated overnight at 37°C. Trypsin was quenched by adding trifluoroacetic acid. The mixture was then subjected to Sep-Pack C18 desalting cartridges (Waters WAT054960). Alternatively, HEK293T cells were transfected with pcDNA3-FLAG-STREP-RNF32. Cells were treated, harvested, and lysed as described above. Whole-cell extracts were used for affinity purification with Strep-Tactin Sepharose resin (Iba 2-1201-002). Proteins were then eluted with Strep-Tactin Elution buffer (Iba 2-1000-025), and the eluate was incubated with anti-FLAG agarose resin and analyzed by mass spectrometry as described above.

CRISPR genome editing

To generate RNF32-/- HCT116 and SW480 cells, three gRNAs targeting exon 1 and exon 8 or exon 1 and exon 7 were designed using the Benchling CRISPR Genome Engineering tool and cloned into pSpCas9(BB)-2A-GFP (PX458). Cells were seeded into 6-well plates at approximately 70% confluency and transfected with 1.25 μg of gRNA-containing PX458 plasmids using TransIT-X2 Transfection reagent (Mirus Bio MIR 6003). Two days after transfection, GFP-positive cells were sorted using the BD FACSAria Fusion cell sorter, and 20 cells/well were plated in a 96-well plate. Two weeks later, single clones were picked, trypsinized in 0.25% Trypsin-EDTA for 5 minutes, and seeded into the individual wells of a 96-well plate for genotyping. Genomic DNA was collected using DNA lysis buffer (100 mM Tris-HCl pH 8.0, 200 mM NaCl, 5 mM EDTA pH 8.0, 0.2% SDS) supplemented with 10 μg/μl proteinase K. Genotyping PCRs were performed with Phusion Taq DNA Polymerase (Thermo Fisher Scientific F530) using primers surrounding the genomic target sites. Positive clones were sequenced to determine the presence of deletion. To further validate the mutational status of candidate clones, single clones were screened for RNF32 expression by qRT-PCR, immunofluorescence and IP-western.

NF-κB luciferase reporter assays

RNF32-/- HCT116 cells seeded in 24-well plates were transfected with pNf-κB-luc and pRL-TK constructs, and, where indicated, with FLAG-HA-tagged RNF32 (wild-type or mutants) with TransIT-X2 transfection reagent (Mirus Bio MIR 6003). Twenty-four hours after transfection, cells were treated with 950 nM ionomycin and 10 ng/ml PMA for 6 hours. Cells were collected, and the relative luciferase activity was measured by the Dual-Luciferase Reporter Assay System according to the manufacturer's instructions (Promega E1910).

Biochemical methods

For preparation of cell extracts, cells were washed and collected in ice-cold PBS and lysed in Triton-X lysis buffer (50 mM Tris pH 7.5, 250 mM NaCl, 0.1% Triton X-100, 1 mM EDTA, 50 mM NaF and protease and phosphatase inhibitors) for 30 minutes on ice, followed by centrifugation for 20 minutes at 4°C. Cell extracts were then submitted to either direct immunoblotting or immunoprecipitation followed by immunoblotting. For immunoprecipitation, cell extracts were first precleared by incubation with protein G- or protein A-Sepharose beads (Thermo Fisher Scientific 101243 and 101042) for 45 minutes at 4°C. Precleared extracts were incubated with the indicated antibody for 3 hours at 4°C, followed by protein G- or protein A-Sepharose beads for 45 minutes. Beads were washed 4 times with lysis buffer, and proteins were eluted in 5x Laemmli sample buffer [50mM Tris-HCl pH 6.8, 2% (w/v) SDS, 5% (v/v) β-mercaptoethanol, 0.1% (w/v) bromophenol blue, and 1% (v/v) glycerol]. For immunoblotting, proteins were separated by SDS-polyacrylamide gel electrophoresis (SDS-PAGE), transferred onto PVDF membranes (Merck-Millipore IPVH00010), and incubated with the indicated antibodies.

For ubiquitylation assay in cultured cells, HEK293T cells were transfected with pcDNA3.1-HA-RNF32 or pcDNA3.1-FLAG-HA-RNF32 (WT or mutants), and pWC7-His-MYC-ubiquitin (WT or mutants). Forty-eight hours later, cells were treated with MG132 for 4 hours before harvesting. Cells were lysed in RIPA buffer (25 mM Tris pH 7.5, 150 mM NaCl, 1% NP40, 1% sodium deoxycholate,

0.1% SDS, and protease and phosphatase inhibitors) and subjected to immunoprecipitation using c-MYC antibody. Ubiquitylated RNF32 was detected by immunoblotting using an anti-HA antibody.

Antibodies

The antibodies raised against the following proteins were used: RNF32 (Merck HPA073560), RNF32 (Abnova H00140545-B02P), FLAG (Merck F7425), FLAG (Merck F3165), HA (Biolegend 901514), HA (Cell Signaling Technology 3724), β-actin (Santa Cruz sc-69879), MYC (Merck M5546), ubiquitin-HRP (Cell Signaling Technology 14049), ubiquitin Lys63-linkage-specific (Merck 05-1308), ubiquitin Lys48-linkage-specific (Merck ZRB2150), ubiquitin Lys48-linkage-specific (Cell Signaling Technology 8081), linear ubiquitin (Merck ZRB2114), Calmodulin (Abclonal A4885), His (Aviva Systems Biology OAEA00010), p-IKKα (Ser176)/p-IKKβ (Ser177) (Cell Signaling Technology 2078), p-IKKα (Ser176)/p-IKKβ (Ser180) (Cell Signaling Technology 2697), Myc (Cell Signaling Technology 2272), Tubulin (Calbiochem CP06), NEMO/IKKγ (Cell Signaling Technology 2685), NEMO/IKKγ (BD Biosciences 611306), IKKα (Santa Cruz Biotechnology sc-7184), IKKβ (Cell Signaling Technology 8943S), p-IκBα (Ser32/36) (Cell Signaling Technology 9246), IκBα (Cell Signaling Technology 4814), NF-κB p65 (Cell Signaling Technology 4764), p27 (BD Biosciences 610242), p21 (Cell Signaling Technology 2947), lysozyme (Abcam ab108508), Ki-67 (Abcam ab15580), and NF-κB p65 (phospho-S536) (Abcam ab86299). For enhanced chemiluminescence (ECL), the detection of proteins was accomplished using the appropriate secondary antibodies conjugated to horseradish peroxidase [anti-mouse IgG (NA931) and anti-rabbit IgG (NA934)] from GE Healthcare.

Quantitative real-time PCR

Total RNA was isolated from wild-type and RNF32-/- HCT116 cells, treated or not with PMA and ionomycin, using the RNeasy Mini Kit (QIAGEN, 74104), and cDNA was synthesized using SuperScript™ II Reverse Transcriptase (Thermo Fisher Scientific, 18064014). The cDNA synthesis was performed according to the manufacturer's instructions, using 2 μg of RNA. For quantitative real-time PCR, amplification was carried out using the GoTaq® qPCR Master Mix (Promega, A6001), according to the manufacturer's protocol in a QuantStudio™ 3 Real-Time PCR instrument (Thermo Fisher Scientific) and the following primer pairs were used: RPLP0-FW ATGTTGCCAGTGTCTGTCTG; RPLP0-REV AGCAAGTGGGAAGGTGTAATC; RNF32-FW GGGTCCTGCAGAAGAATAGAAG; RNF32-REV CTGCATTGACTGCCAAGTTATC; NFKBIA-FW CTCCGAGACTTTCGAGGAAATAC and NFKBIA-REV CCATTGTAG TTGGTAGCCTTCA. Gene expression levels were quantified using the ΔΔCt method, and RPLP0 was used as the housekeeping gene for normalization.

RNA Sequencing

Total RNA was extracted from wild-type and RNF32-/- HCT116 cells, treated or not with PMA and ionomycin, using the RNeasy Mini Kit (QIAGEN, Catalog No. 74104), following the manufacturer's protocol. RNA sequencing was conducted by Macrogen Europe B.V. (Amsterdam, Netherlands) on an Illumina NovaSeq X 100 PE, generating 150 bp paired-end reads. The sequencing depth was approximately 100 million reads per sample. The raw sequencing data were obtained in FASTQ format. The raw sequencing data were processed using FastQC (v0.11.9) to assess the quality of the reads, and Trimmomatic was used to trim adapters and low-quality bases. Reads were then aligned to the hg38 reference genome using HISAT2. Gene expression levels were quantified by counting reads mapped to exonic regions using featureCounts based on the GENCODE human gene annotation. Differential gene expression analysis was performed using DESeq2 with default settings. Genes with a log2 fold change ≥ 2 and an adjusted p-value (FDR) < 0.05 were considered significantly differentially expressed.

Immunofluorescence

Cells were seeded on poly-L-lysine (Merck P4707) coated glass coverslips and, when specified, transfected with the indicated plasmids. One day after transfection, cells were washed with PBS and fixed with 4% paraformaldehyde in PBS for 15 minutes at RT. Cells were then permeabilized with 0.1% Triton X-100 in PBS for 10 minutes at RT. To analyze cellular condensates, cells were permeabilized with 0.02% saponin in PBS for 3 minutes at room temperature before the fixation step. Fixed cells were blocked in 5% BSA in PBS for 1 hour and then incubated with primary antibodies for 2 hours at room temperature or overnight at 4°C. Cells were washed three times using PBS and incubated with Alexa Fluor 488 (A11029), Alexa Fluor 568 (A10042), Alexa Fluor 594 (A11005), or Alexa Fluor 488 (A21206) conjugated secondary antibodies (Thermo Fisher Scientific) for 1 hour at room temperature. Cells were washed three times with PBS, and slides were mounted using the ProLong™ Gold Antifade Mountant with DAPI (Thermo Fisher Scientific P36935). Fluorescence images were acquired on a Leica DM2500 fluorescence microscope and analyzed using the ImageJ software. RNF32 puncta were quantified by counting the number of 0.3-1 μm puncta and using the cell counter module of ImageJ. The colocalization plugin in ImageJ was used to visualize colocalization between two channels (thresholds were set equal for all images analyzed).

In vitro binding assay

In vitro translated HA-tagged RNF32 (TNT Quick Coupled Transcription/Translation System – Promega L1170) was incubated with human Calmodulin-Sepharose 4B beads (Cytiva 17052901) for 1 hour at 4°C in buffer (150 mM NaCl, 25 mM Tris HCl pH 7.5, 0.1% NP-40) containing either 2 mM $CaCl_2$ or 5 mM EGTA. Beads were washed three times with the same buffer. Proteins were then eluted with Laemmli buffer for 3 minutes at 95°C and subjected to SDS-PAGE and immunoblotting.

Calmodulin production and RNF32 peptide synthesis

Human recombinant calmodulin was purified as described previously.[38] The RNF32 peptide (188-KCVTRIQAYWRGCVVRK WYRNLR-210) was synthesized by GenScript Inc. The peptide concentration was determined using its predicted molar extinction coefficient at 280 nm. The mobility shift of CaM induced by RNF32p was assessed under native conditions on a 12.5% continuous gel containing 2 mM $CaCl_2$, following the procedure described in.[39,40] Fluorescence spectra were recorded on a Jasco FP8200 spectrofluorometer. The Trp residues of RNF32 were selectively excited at 295 nm, and fluorescence emission was recorded from 305 to 500 nm in the absence and presence of CaM in a buffer containing 50 mM Hepes, 150 mM KCl pH 7.5, and 2 mM $CaCl_2$.

AlphaFold2-Multimer prediction

The computational resources of the IFOM-ETS cluster were used to run AlphaFold2 leveraging on the nf-core[41] pipeline: proteinfold 1.1.0dev (revision c246c853c6); the databases described in[18] were used for the predictions. The top-ranking structure from 25 predicted structures was selected for visualization and display. Structures were analyzed, and figures were generated by using PyMol (PyMOL Molecular Graphics System, Version 2.3.5 Schrödinger, http://www.pymol.org).

Time-lapse confocal imaging

Cells were grown on glass-bottom dishes to 70% confluency and transfected with the pEGFP-RNF32 plasmid. Cells were stimulated with 950 nM ionomycin and 10 ng/ml PMA 24 hours after transfection. Confocal live cell image series were acquired with a Nikon A1R confocal microscope with a 20x NA 0.75 Plan Apo VC objective. All experiments were conducted at 37°C and 5% CO2 using a stage incubation system (OkoLab) and an Eclipse Ti-E inverted microscope (Nikon) equipped with a built-in Perfect Focus System. 489.1 nm diode laser was used for the excitation of GFP and set at 3.3% to minimize the possible phototoxic effects induced by fluorescence illumination on live cells. The fluorescence emission was collected at 525/50 nm with a PMT detector. The diameter of the detection pinhole was set at 2.5 Airy Unit (69 μm) to generate a single thick optical section passing through the center of the cells. Sequential images of 512 x 512 pixels at 12 bits (4096 grey levels) were collected at a fixed pixel size of 63 μm every 60 seconds for 3 hours. Transmission and fluorescence images were merged and rendered using NIS Elements Advanced Research software (Nikon). The fluorescence intensity over time was assessed across the entire frame with a minimum of 4-point sets for each tested condition. Values were normalized for comparison between treated and untreated samples.

Optical diffraction tomography

The distribution of GFP-RNF32 in cells was examined utilizing a holotomography (HT) microscope (Tomocube HT-X1TM; Tomocube Inc., Korea) as previously described.[42] This HT system enabled comprehensive capture of both the 3D refraction index (RI) dispersion and three-channel 3D fluorescence imaging, achieved through multiple 2D hologram images from various illumination angles. The system highlighted a resolution of 156 nm laterally and 1070 nm axially for the refraction index, while fluorescence optical resolution stood at 270 nm laterally and 1130 nm axially at a wavelength of 488 nm. Live-cell imaging was analyzed using Olympus UPLXAPO 40×, NA 0.95, air objective lens. The fluorescence image step size was set to be the same as the HT imaging step size. TomoStudioTM software version X 1.6 (Tomocube Inc., Korea) was utilized for visualization and analysis of the 3D distribution of refractive index and fluorescence in live cells.

Fluorescence recovery after photobleaching

FRAP experiments were performed at 37°C in a live-cell-imaging dish using a Nikon A1R confocal microscope with a 60× NA 1.4 Plan Apo VC oil immersion objective. GFP was bleached in a region of interest (ROI, 5 x 5 μm) using 100% laser power at 489.1 nm. Prebleach and recovery images were recorded with a pinhole size of 233 um for the indicated time. Fluorescence intensity was measured using NIS Elements Advanced Research software (Nikon) in both bleached and control ROI.

Confocal and colocalization analysis

Confocal analysis was performed using a Nikon A1 confocal laser scanning microscope with a 100× NA 1.49 objective lens and 408, 489, and 562 nm laser lines. Z-stacks were collected at an optical resolution of 100 nm/pixel and stored at 12-bit with 4096 different gray levels, with pinhole diameter set to 1 Airy unit and z-step size set to 300 nm. Confocal images were processed using the Richardson-Lucy deconvolution algorithm using NIS-Elements Advanced Research software (Nikon). A large area of the samples was observed, and 5 representative cells for each condition were analyzed and processed as described thereafter.

Colocalization analysis was evaluated by comparing the equivalent pixel positions of blue and red signals of fluorophores in each of the acquired images (optical sections). A two-dimensional scatter plot diagram of the individual pixels from the paired images was generated, and a threshold signal level to be included in the analysis was selected. Pixels with intensity values greater than 50% gray levels (on a scale from 0 to 4096) were selected for both signals and the colocalization binary maps that indicate regions containing highly colocalized signals were imaged and merged (in white) to the green and red signals.[43,44] The measurements using single optical sections through the middle of the nucleus. The analysis of the images was carried out using NIS-Elements HC software version 5.20 (Nikon). The colocalization of the fluorochromes was quantified using Pearson's colocalization coefficient (r) derived from 90 analyzed optical sections and expressed as a percentage ± SD.

Azoxymethane (AOM)/Dextran Sodium Sulfate (DSS) mouse model

Colitis-associated colorectal tumors were induced as previously described[45] with minor modifications. Briefly, Rnf32-/- mice and their littermate controls (C57BL/6J background), all males of 8–12 weeks of age, were used in this study. Mice were housed under specific pathogen-free conditions with free access to food and water. On day 0, mice received a single intraperitoneal (i.p.) injection of azoxymethane (AOM; MP Biomedicals, Cat# 183971) at a dose of 10 mg/kg body weight. After a one-day recovery period, 2.5% dextran sulfate sodium (DSS; MP Biomedicals, Cat# 160110) was provided in the drinking water for 7 consecutive days, followed by 10 days of regular water. This DSS treatment cycle was repeated two additional times (a total of three cycles). Mice were monitored daily for weight loss and survival. At day 120, animals were euthanized, and the entire colon was excised, flushed with PBS, and examined for macroscopic tumors. Tumor number was counted, and tumor size (area) was measured from colon images using ImageJ software (NIH, Bethesda, MD). Tissues were fixed in 10% neutral-buffered formalin or frozen for further analysis.

Analysis of small intestinal organoids

For histological analysis, organoids were cultured in IntestiCult™ Organoid Growth Medium (STEMCELL Technologies). Once grown, organoids were harvested, fixed by 4% PFA for 1 hour, embedded in 2% agarose gel, and then processed for paraffin embedding. For protein analysis, organoids were lysed using cold lysis buffer (50 mM pH 7.5 Tris-HCl, 250 mM NaCl, 0.1 % Triton X-100, 1 mM EDTA, 50 mM NaF) with protease inhibitor cocktail (Nacalai Tesque Inc., Kyoto, Japan) and processed for immunoblotting analysis.

In silico analysis of RNF32 expression in cancer

RNF32 mRNA expression of tumoral and adjacent-normal tissues for BLCA (bladder urothelial carcinoma), BRCA (breast invasive carcinoma), CESC (cervical squamous cell carcinoma and endocervical adenocarcinoma), CHOL (cholangiocarcinoma), COAD (colon adenocarcinoma), ESCA (esophageal carcinoma), HNSC (head and neck squamous cell carcinoma, KIRC (kidney renal clear cell carcinoma), KIRP (kidney renal papillary cell carcinoma), LUAD (lung adenocarcinoma), PAAD (pancreatic adenocarcinoma), PCPG (pheochromocytoma and paraganglioma), PRAD (prostate adenocarcinoma), READ (rectum adenocarcinoma), STAD (stomach adenocarcinoma), THYM (thymoma) and UCEC (uterine corpus endometrial carcinoma) was obtained from TCGA datasets through the UCSC Xena browser (http://xena.ucsc.edu/ – IlluminaHiSeq gene expression RNAseq normalized data). Statistical analysis was performed using the computing environment Python: non-parametric Mann-Whitney U tests were used to analyze differences among RNF32 mRNA expression levels in primary tumors versus normal adjacent tissues, and the Log-Rank (Mantel-Cox) test was used to compare overall survival curves in patients with primary tumors with low or high RNF32 mRNA expression. One-way ANOVA and Tukey tests were used to analyze RNF32 expression across COAD stages. Cox's proportional hazard model was used to evaluate the association of RNF32 expression with survival time, using covariates (age at diagnosis, gender, histological subtypes, and RNF32 status). $p < 0.05$ were considered significant.

QUANTIFICATION AND STATISTICAL ANALYSIS

All data represent the average from at least three independent experiments, except where specified in figure legends. Sample sizes and p values are indicated in figure legends.

Molecular Cell, Volume *85*

Supplemental information

The E3 ligase RNF32 controls the IkB kinase complex and NF-kB signaling in intestinal stem cells

Angela Lauriola, Juliana Haydeé Enriqué Steinberg, Motoharu Sarubo, Elena Maspero, Fabiana Alejandra Rossi, Yasuhiro Mouri, Marco Pedretti, Mohsen Hajisadeghian, Vincenzo Taibi, Andrea Vettori, Nicola Vitulo, Michael Assfalg, Mariapina D'Onofrio, Mario Rossi, Akihiro Yasue, Alessandra Astegno, Simona Polo, Spartaco Santi, Yasusei Kudo, and Daniele Guardavaccaro

A

E3 classes	#
F-box and WD repeat domain (FBXWs) proteins	11
F-box and leucine rich repeat (FBXLs) proteins	21
F-box other (FBXOs) proteins	39
SOCS box proteins	27
BTB proteins	134
DDB1 and CUL4 associated factors (DCAF)	24
RING finger proteins (RNFs)	303
RING-in-between-RING (RBR)	14
Linear ubiquitin chain assembly complex	3
HECT ubiquitin ligases	13
Pellino E3 ubiquitin protein ligases (PELI)	3
Ubiquitin protein ligase E3 component n-recognins (UBR)	7
Various E3 ubiquitin ligases	56
Total	**655**

B

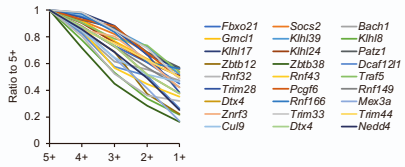

Figure S1. Gene expression profile of 655 E3 ubiquitin ligases in intestinal stem cells, related to Figure 1.
(A) Classes of E3 ubiquitin ligases whose expression was analyzed in intestinal stem cells. The number of analyzed E3s belonging to each class is shown.
(B) Graph of the expression profile of genes encoding for E3 ubiquitin ligases. Crypt cells were sorted on the basis of LGR5-GFP expression into five fractions (highest in fraction 5+), and microarray expression profiling was carried out. Each sample was compared to sample 5+.

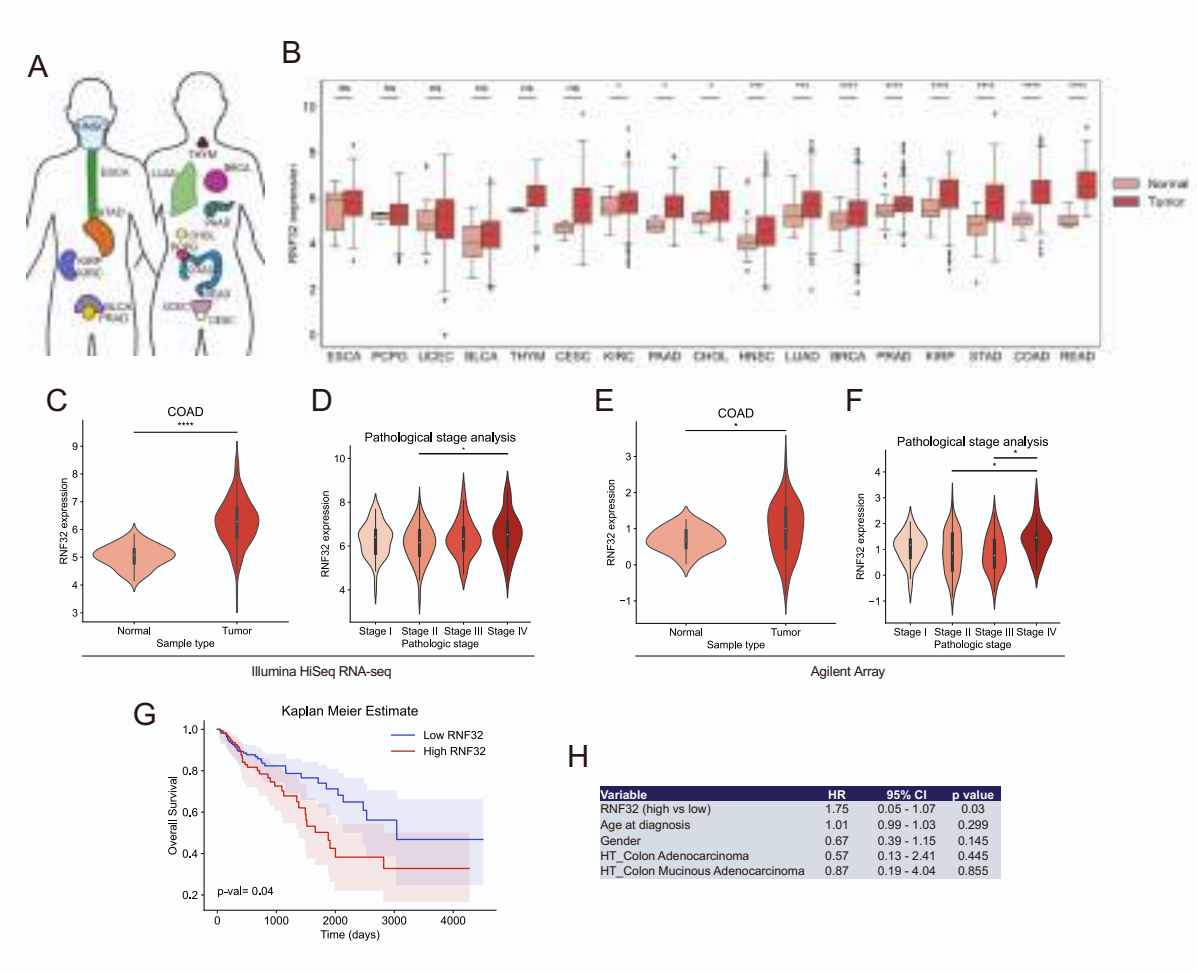

Figure S2. RNF32 expression is increased, and correlates with poor prognosis, in human colorectal cancer, related to Figure 1.

(A) Schematic illustration of the human cancer types included in the transcriptomic analysis of RNF32 gene expression. The abbreviations of the Cancer Genome Atlas Program (TCGA) study are as follows: BLCA (bladder urothelial carcinoma), BRCA (breast invasive carcinoma), CESC (cervical squamous cell carcinoma and endocervical adenocarcinoma), CHOL (cholangiocarcinoma), COAD (colon adenocarcinoma), ESCA (esophageal carcinoma), HNSC (head and neck squamous cell carcinoma), KIRC (kidney renal clear cell carcinoma), KIRP (kidney renal papillary cell carcinoma), LUAD (lung adenocarcinoma), PAAD (pancreatic adenocarcinoma), PCPG (pheochromocytoma and paraganglioma), PRAD (prostate adenocarcinoma), READ (rectum adenocarcinoma), STAD (stomach adenocarcinoma), THYM (thymoma) and UCEC (uterine corpus endometrial carcinoma).

(B) Boxplot analysis of RNF32 expression across various human primary tumors. The boxes refer to the quantile distribution (25–75%) range of relative RNF32 mRNA levels [TCGA RNAseq data expressed as $\log_2$ (norm_count + 1)] with the median shown as black horizontal lines. Non-parametric Mann-Whitney U tests were used to analyze difference significance (*p < 0.05; **p < 0.01; ***p < 0.001; ****p < 0.0001).

(C-F) Analysis of RNF32 expression in COAD (TCGA datasets). IlluminaHiSeq gene expression RNAseq normalized data expressed as log2 (norm_count + 1) (C and D) as well as gene level transcription estimates by Agilent array, as log2 lowess normalized ratio of sample signal to the reference signal (cy5/cy3) collapsed by gene (E and F) are shown. (C) Analysis of RNF32 expression in COAD primary tumors and adjacent normal tissue (p = 1.07e-17). (D) Analysis of RNF32 expression across tumor samples at different stages of COAD showing a positive relation between RNF32 and COAD disease progression (Stage II vs Stage IV p = 0.0246). (E) Analysis of RNF32 expression in COAD primary tumors and adjacent normal tissue (p = 0.04). (F) Analysis of RNF32 expression across tumor samples at different stages of COAD showing a positive relation

between RNF32 expression and COAD disease progression (Stage II vs Stage IV p = 0.0149; Stage III vs Stage IV p = 0.0403).

(G) Kaplan–Meier estimates of overall survival (OS) in patients with colorectal cancer according to low RNF32 mRNA levels (blue line, n = 170) and high RNF32 mRNA levels (red line, n = 113). Low/high RNF32 expression samples were divided using quantile = 0.6 as a threshold, and survival curve difference significance was determined using the Log-Rank (Mantel-Cox) test (p = 0.04). Median survival for low and high groups was 3042 and 1881 days, respectively.

(H) $RNF32^{High}$ expression is an independent prognostic predictor of OS. Multivariate analysis of RNF32 expression in COAD tumors indicated that $RNF32^{High}$ is an independent prognostic predictor of OS. HR: Hazard Ratio, CI: Confidence Interval (n = 271, Cox's proportional hazard model, OS p = 0.03).

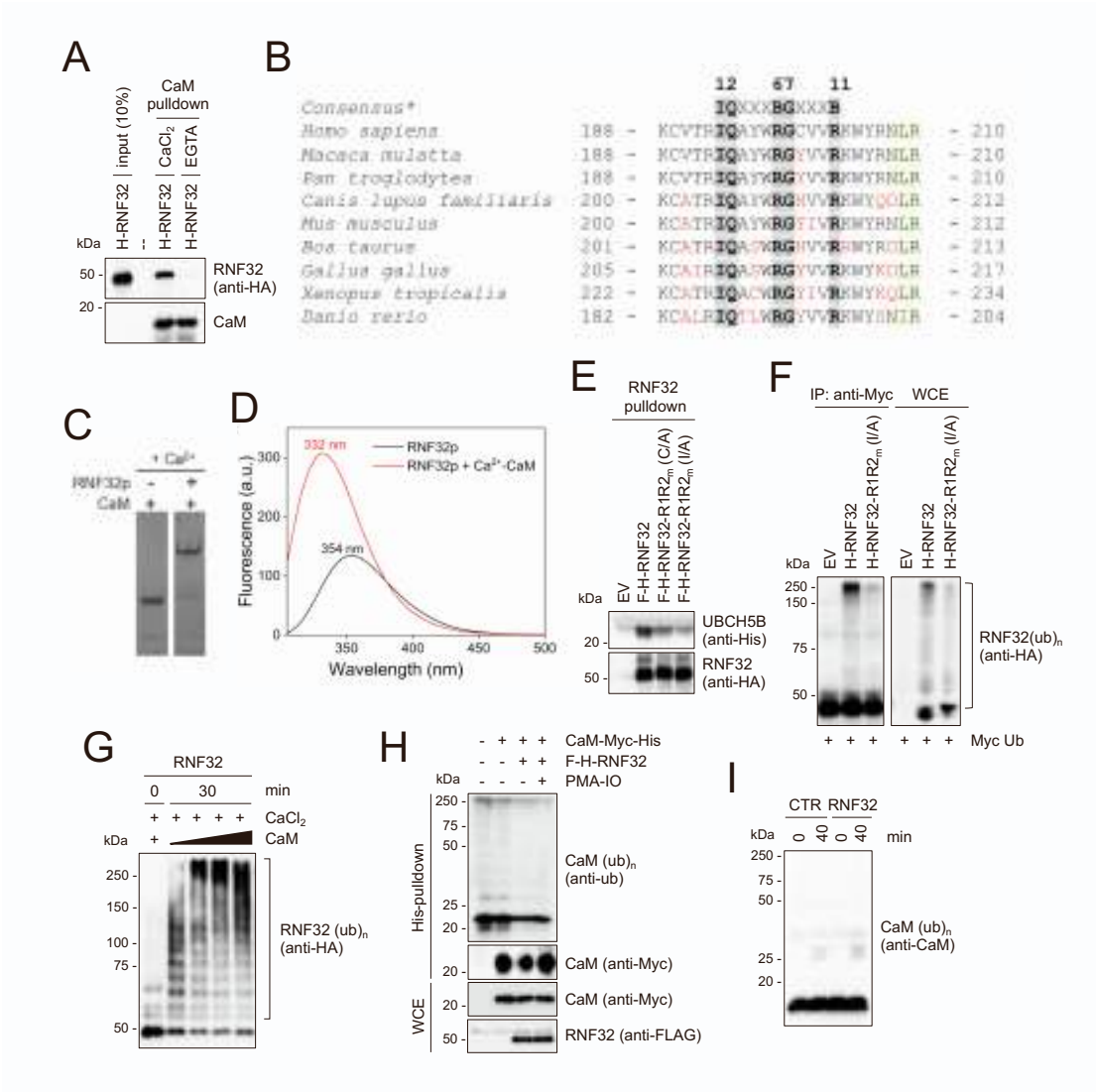

Figure S3. Characterization of the interaction between RNF32 and Calmodulin, related to Figure 1.

(A) Ca^{2+}-dependent binding of Calmodulin (CaM) to RNF32 in vitro. HA-RNF32 was transcribed/translated in vitro and incubated with Sepharose-4B beads coupled to human CaM in the presence of either 2 mM $CaCl_2$ or 5 mM EGTA. After washing, beads were analyzed by immunoblotting with an anti-HA antibody to reveal CaM-bound RNF32.

(B) Sequence alignment of the IQ motif from RNF32 orthologs. The consensus sequence of the IQ motif is also shown.

(C) Binding of CaM to the RNF32p peptide on native PAGE in the presence of 2 mM $CaCl_2$.

(D) Steady-state Trp fluorescence analysis. Trp fluorescence emission spectra of RNF32p alone (black line), and upon addition of CaM (red line) in the presence of 2 mM $CaCl_2$.

(E) In vitro pulldown of immunopurified RNF32 (wild-type or the indicated mutants) with recombinant UBCH5B.

(F) As in Figure 1I, except that cells were transfected with FLAG-HA-tagged wild-type RNF32, RNF32(I129A/I295A) (RNF32-R1R2$_m$ I/A), or an empty vector (EV).

(G) In vitro ubiquitin ligation assay of immunopurified FLAG-HA-tagged RNF32 was carried out in the presence of purified recombinant E1, UBCH5B, wild-type ubiquitin, and increasing concentrations of purified recombinant CaM. Samples were resolved by SDS-PAGE and probed with an anti-HA antibody. The bracket on the right side indicates a ladder of bands corresponding to polyubiquitylated RNF32.

(H) HEK293T cells were transfected with His-Myc-tagged CaM and FLAG-HA-tagged RNF32 and treated with 10 ng/ml PMA and 950 nM ionomycin for 60 minutes as indicated. Cells were lysed in denaturing

conditions, and WCEs were subjected to a His-pulldown. Purified complexes were then analyzed with the indicated antibodies.
(I) In vitro ubiquitin ligation assay of purified recombinant CaM was performed in the presence of purified recombinant E1, UBCH5B, ubiquitin, with or without in vitro translated RNF32. Samples were resolved by SDS-PAGE and analyzed by immunoblotting with an anti-CaM antibody.

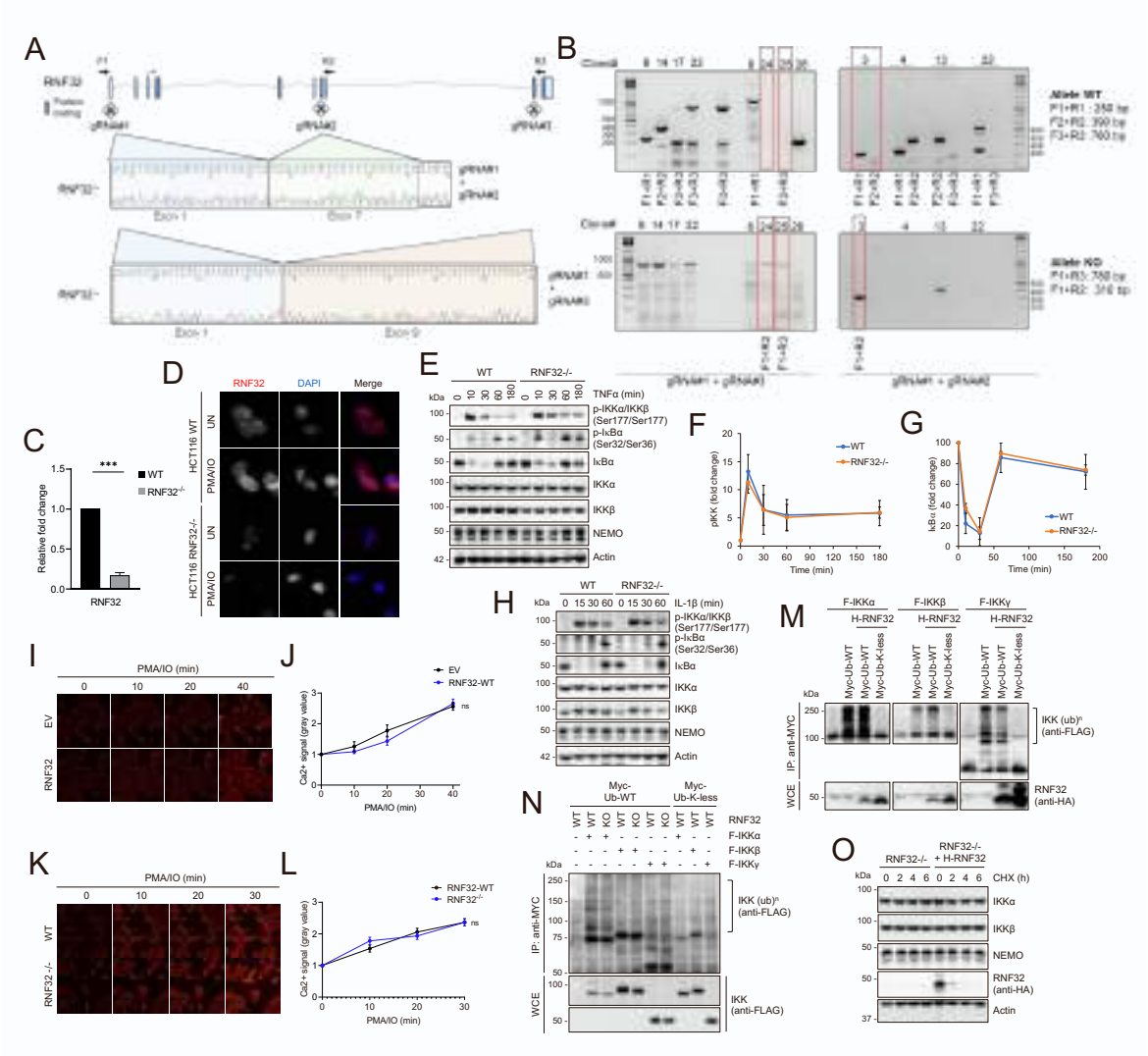

Figure S4. RNF32 is not required for NF-κB activation in response to TNFα or IL-1β, related to Figure 2.

(A) Schematic representation of the CRISPR/Cas9 strategy used to delete the RNF32 gene in HCT116 cells. Empty rectangles indicate exons, filled rectangles represent the coding exons. gRNA#1, gRNA#2, and gRNA #3 indicate the three gRNAs that were used in two different combinations: gRNA#1 and gRNA#3 (exon 1 and exon 9) and gRNA#1 and gRNA#2 (exon 1 and exon 7). Chromatograms display the results of sequencing runs.

(B) Genomic DNA samples were genotyped by PCR. The knockout (KO) alleles obtained after using the gRNA#1 and gRNA#3 or gRNA#1 and gRNA#2 combinations are indicated in red rectangles with a band size of 780 bp or 310 bp, respectively.

(C) Relative expression levels of RNF32 were measured by quantitative real-time PCR (qPCR) in HCT116 wild-type (WT) and RNF32 knockout (RNF32-/-) cells.

(D) Parental and RNF32-/- HCT116 cells, stimulated with 10 ng/ml phorbol-12-myristate-13-acetate (PMA) and 950 nM ionomycin (IO) for 90 minutes or left untreated, were immunostained with an anti-RNF32 antibody to validate the knockout of RNF32.

(E-G) Parental or RNF32-/- HCT116 cells were treated with 20 ng/ml TNFα for the indicated times. Cells were lysed, and total cell extracts were analyzed by immunoblotting with antibodies specific for the indicated proteins (E). The graphs show the quantification of phospho-IKKα/IKKβ (F) and IκBα (G) levels as shown in E.

(H) Parental or RNF32-/- HCT116 cells were treated with 1 ug/ml IL-1β for the indicated times. Cells were lysed, and total cell extracts were analyzed by immunoblotting with antibodies specific for the indicated proteins.
(I-J) Control or RNF32 overexpressing HEK293T cells were treated with the live cell red fluorescent calcium indicator Biotracker 609 Red Ca^{2+} AM Dye for the indicated time, and the intensity of this fluorescent probe was measured by microscopy (I). The graph shows the mean ± s.e.m. (n = 15 cells) for each time point (J). ns = not significant.
(K-L) As in I-J, except that wild-type and RNF32-/- HCT116 cells were analyzed.
(M) RNF32 does not trigger ubiquitylation of IKKα, IKKβ, and NEMO. HEK293T cells were transfected with HA-tagged RNF32, MYC-tagged ubiquitin (wild-type [WT] or lysine-less [Lys-less]), with or without FLAG-tagged IKKα, FLAG-tagged IKKβ or FLAG-tagged NEMO. Cells were lysed in denaturing buffer, and whole cell extracts (WCE) were immunoprecipitated with an anti-MYC antibody. Immunoprecipitates were then immunoblotted with an anti-FLAG antibody to detect ubiquitylated IKK proteins.
(N) Parental or RNF32-/- (KO) HCT116 cells were transfected with MYC-tagged ubiquitin (wild-type [WT] or lysine-less [Lys-less]), with or without FLAG-tagged IKKα, IKKβ or NEMO. Cells were lysed in denaturing buffer, and WCEs were immunoprecipitated with an anti-MYC antibody. Immunoprecipitates were then immunoblotted with an anti-FLAG antibody.
(O) RNF32-/- HCT116 cells or RNF32-/- HCT116 cells re-expressing wild-type RNF32 were treated with cycloheximide. At the indicated times, cells were collected and analyzed by immunoblotting with antibodies specific for the indicated proteins.

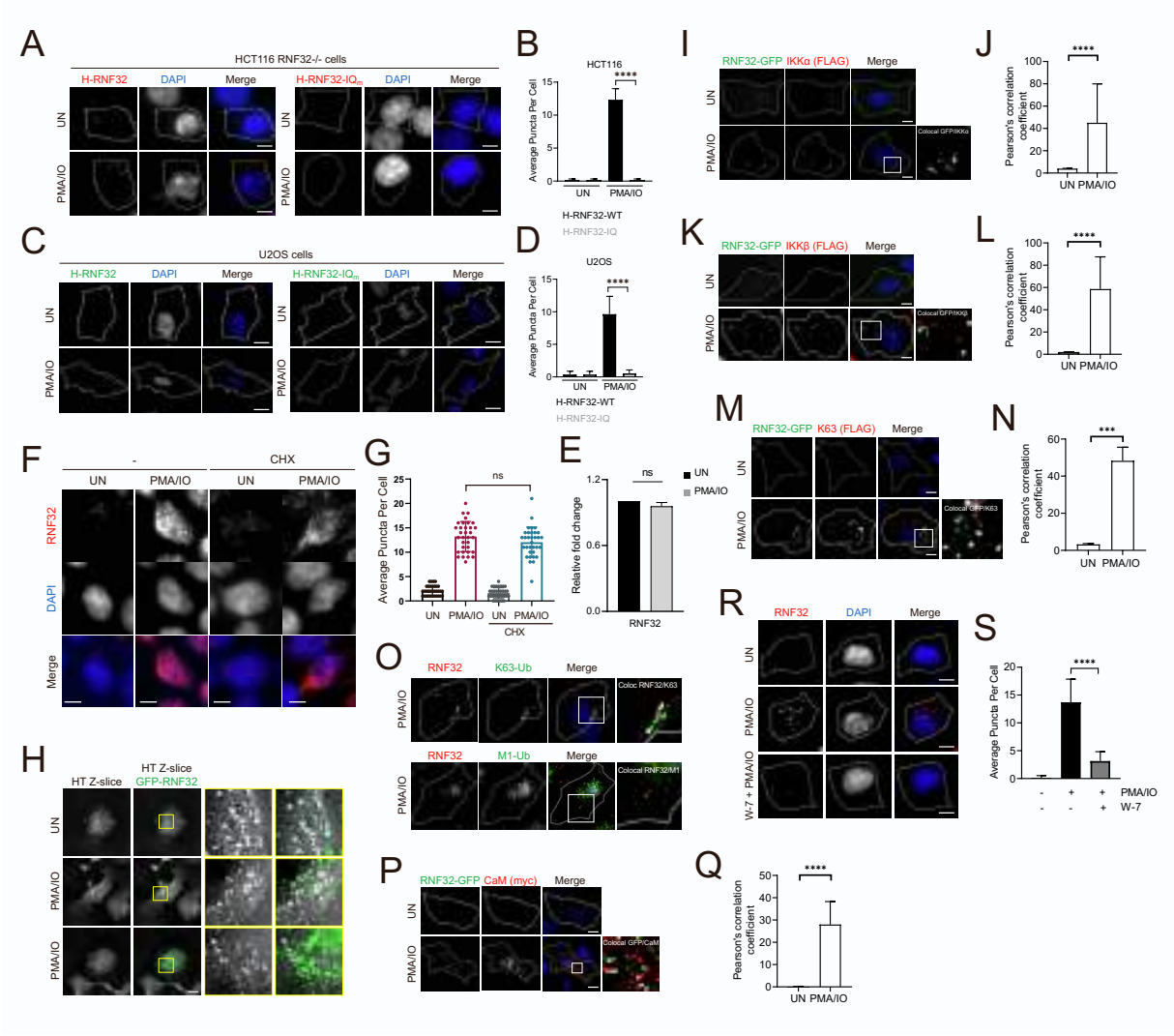

Figure S5. RNF32 forms liquid-like condensates, related to Figure 3.

(A) RNF32-/- HCT116 cells re-expressing (by lentiviral transduction) either HA-tagged wild-type RNF32 or RNF32-IQ_m were stimulated with 10 ng/ml PMA and 950 nM ionomycin or left untreated. Cells were then fixed and immunostained for HA. Scale bars indicate 10 µm.

(B) Quantification of RNF32 puncta per cell as shown in A. Means ± s.e.m. are shown (n = 15 cells). Unpaired t-test. ****$p < 0.0001$.

(C) U2OS expressing either HA-tagged wild-type RNF32 or the RNF32-IQ_m mutant were stimulated with 10 ng/ml PMA and 950 nM ionomycin or left untreated. Cells were then fixed and immunostained for HA. Scale bars indicate 10 µm.

(D) Quantification of RNF32 puncta per cell as shown in C. Means ± s.e.m. are shown (n = 15 cells). Unpaired t-test. ****$p < 0.0001$.

(E) Relative RNF32 mRNA levels measured by qRT-PCR in HCT116 cells treated with 10 ng/ml phorbol-12-myristate-13-acetate (PMA) and 950 nM ionomycin (IO) for 90 minutes.

(F) Immunofluorescence staining of endogenous RNF32 in HCT116 cells treated with cycloheximide (CHX) to inhibit protein synthesis and stimulated for 90 minutes with 10 ng/ml phorbol-12-myristate-13-acetate (PMA) and 950 nM ionomycin (IO) or left untreated (UN). Scale bars indicate 10 µm.

(G) Quantification of average numbers of RNF32 puncta per cell as shown in F. Means ± s.e.m. n = 30 cells). Unpaired t-test. n.s., $p > 0.05$.

(H) Label-free holotomographic Z-slice and fluorescence imaging of U2OS cells expressing wild-type GFP-RNF32 and treated with 10 ng/ml phorbol-12-myristate-13-acetate (PMA) and 950 nM ionomycin (IO) for 90

minutes or left untreated. Images were acquired with a holotomography (HT) microscope. Insets show magnified images. Scale bar: 10 μm.

(I) U2OS expressing wild-type RNF32-GFP and FLAG-IKKα were stimulated with 10 ng/ml PMA and 950 nM ionomycin or left untreated. Cells were then fixed and immunostained for FLAG. Scale bars indicate 10 μm.

(J) Quantification of the colocalization as shown in I using Pearson's colocalization coefficient expressed as percentage ± s.e.m. n = 5 cells. ****p < 0.0001.

(K-L) As in I-J, except that IKKβ was expressed instead of IKKα.

(M-N) As in I-J, except that FLAG-ubiquitin(K63only) was expressed instead of FLAG-IKKα. This Ubiquitin mutant contains only a single lysine, K63, with all other lysine residues mutated to arginine.

(O) U2OS were stimulated with 10 ng/ml PMA and 950 nM ionomycin. Cells were then fixed and immunostained for RNF32 and either Lys63- or Met1-linked ubiquitin chains.

(P-Q) As in I-J, except that MYC-CaM was expressed instead of IKKα.

(R) Immunofluorescence staining of endogenous RNF32 in U2OS cells stimulated with 10 ng/ml phorbol-12-myristate-13-acetate (PMA) and 950 nM ionomycin (IO) for 90 minutes with or without the CaM inhibitor W-7. Scale bars indicate 10 μm.

(S) Quantification of average numbers of RNF32 puncta per cell as shown in R. Means ± s.e.m. n = 10 cells. Unpaired t-test ***p < 0.0001.

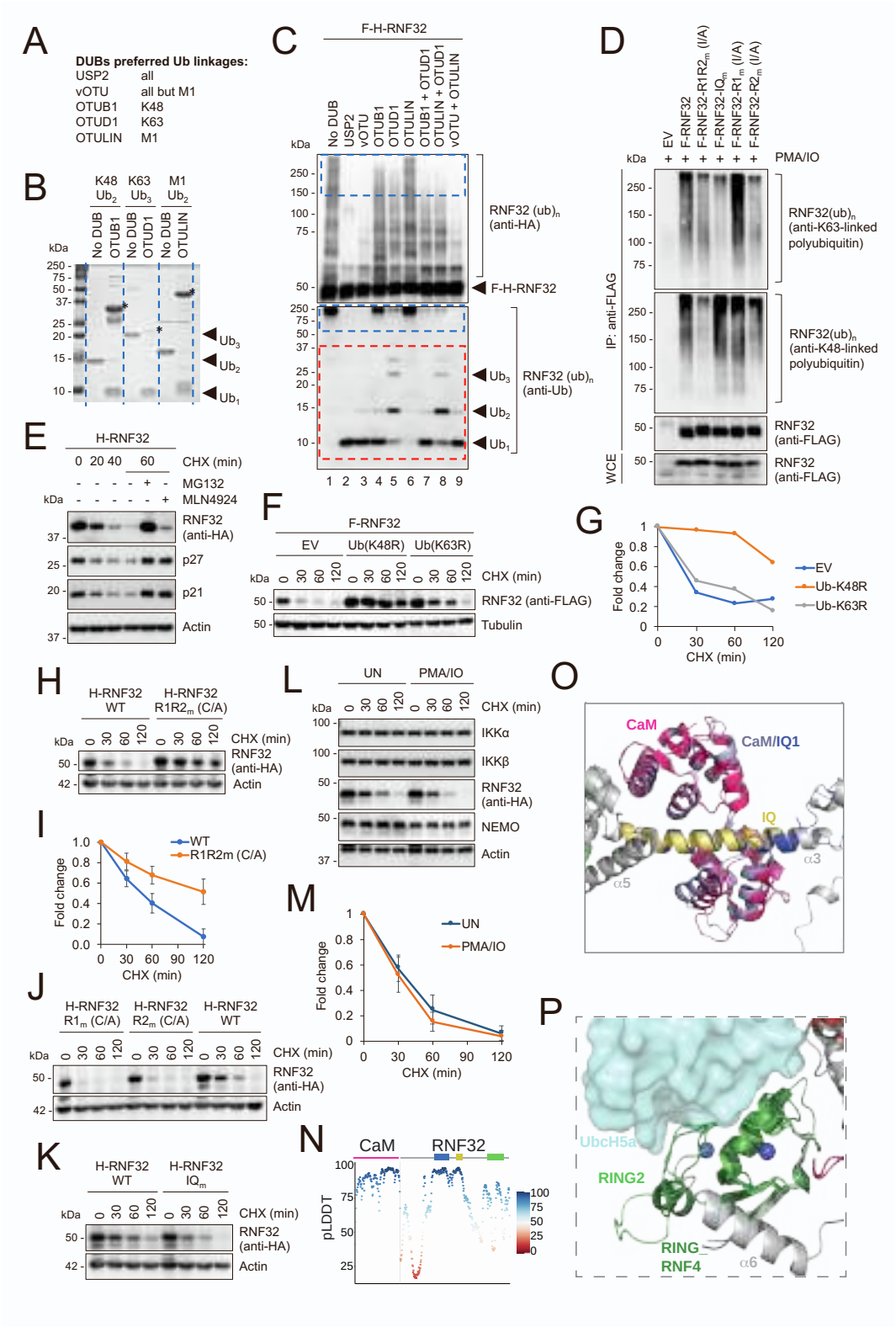

Figure S6: Regulation of RNF32 ubiquitylation and turnover, related to Figure 4.

(A) The purified DUBs and their preferred ubiquitin linkages that were utilized for the UbiCRest analysis of RNF32 autoubiquitylation.

(B) DUB specificity analysis. The indicated purified DUBs were incubated with Lys48-linked diubiquitin, Lys63-linked triubiquitin, or Met1-linked diubiquitin for 60 minutes. The reactions were subjected to SDS-PAGE, and gels were stained with Coomassie blue. Asterisks point to the purified DUBs employed in the reactions.
(C) FLAG-HA-epitope tagged RNF32, immunoprecipitated from HEK293T cells treated with 10 ng/ml phorbol-12-myristate-13-acetate (PMA) and 950 nM ionomycin for 90 minutes, was incubated with the indicated DUBs, alone or in combination. Reactions were then subjected to immunoblotting with anti-HA and anti-ubiquitin antibodies.
(D) HEK293T cells were transfected with FLAG-tagged wild-type RNF32 or the indicated mutants and treated with 10 ng/ml PMA and 950 nM ionomycin for 90 minutes. Cells were lysed in denaturing conditions, and WCEs were immunoprecipitated with an anti-FLAG antibody. Immunoprecipitates were then immunoblotted with Lys63 (top) or Lys48 (middle) linkage-specific anti-ubiquitin antibodies. The brackets on the right side mark a ladder of bands corresponding to polyubiquitylated RNF32.
(E) HEK293T cells transfected with HA-tagged RNF32 (H-RNF32) were treated with the inhibitor of protein synthesis cycloheximide (CHX) for the indicated times with or without MG132 (proteasome inhibitor) or MLN4924 (Cullin-RING E3 inhibitor). Cells were then collected and analyzed by immunoblotting.
(F) HEK293T cells transfected with HA-tagged RNF32 (H-RNF32) and ubiquitin(K48R), ubiquitin(K63R), or an empty vector (EV) were treated with cycloheximide. At the indicated times, cells were collected and analyzed by immunoblotting.
(G) The graph shows the quantification of RNF32 expression as shown in F.
(H) RNF32-/- HCT116 cells were transduced with lentivirus expressing FLAG-HA-tagged wild-type RNF32 or the RNF32-R1R2$_m$ (C/A) mutant and treated with cycloheximide. At the indicated times, cells were collected and analyzed by immunoblotting.
(I) The graph shows the quantification of RNF32 expression as shown in H.
(J) as in H, except that the RNF32-R1$_m$ (C/A) mutant or the RNF32-R2$_m$ (C/A) mutant were transduced in RNF32-/- HCT116 cells.
(K) As in H, except that the RNF32-IQ$_m$ mutant was transduced in RNF32-/- HCT116 cells.
(L) As in H, except that parental cells were treated with PMA and ionomycin or left untreated.
(M) The graph shows the quantification of RNF32 expression as shown in L.
(N) Predicted Local distance difference test (pLDDT) for CaM:RNF32 complex generated by AlphaFold2.
(O) Cartoon representation of the superposition of apo-CaM:IQ1 domain of Myosin V (PDB:2IX7) with the CaM:RNF32 complex generated by AlphaFold2. Apo-CaM is in light blue, IQ1 in blue, CaM is in dark pink, the IQ domain of RNF32 is in yellow.
(P) Cartoon representation of the superposition of RNF4 RING–UbcH5A–Ub complex (PDB: 4AP4) with the AlphaFold2 prediction of the CaM:RNF32 complex, corresponding to the dashed rectangle in Figure 4H. Superposition was done by aligning RING2 (light green) with the RING of RNF4 (dark green). UbcH5a is shown in cyan.

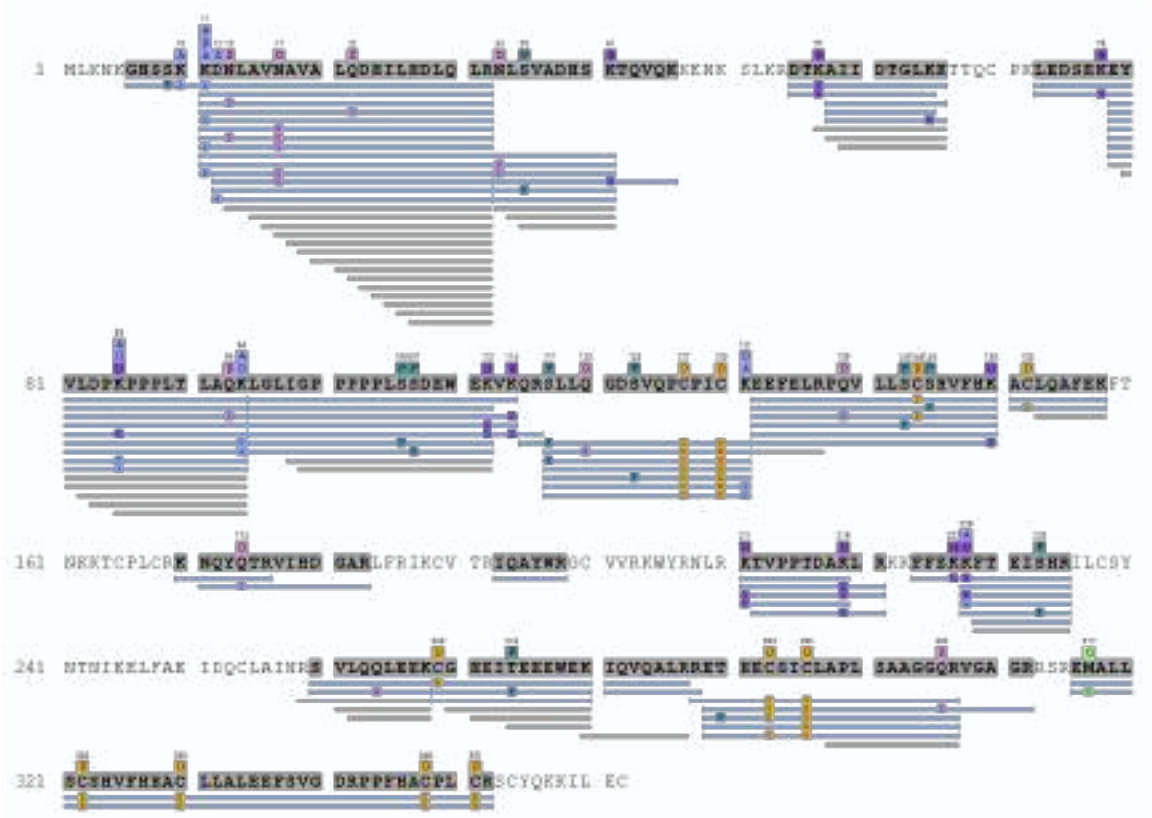

Figure S7: RNF32 post-translational modifications, related to Figure 4.
RNF32 was immunopurified and analyzed by mass spectrometry. The recovered RNF32 peptides and their post-translational modifications are shown.

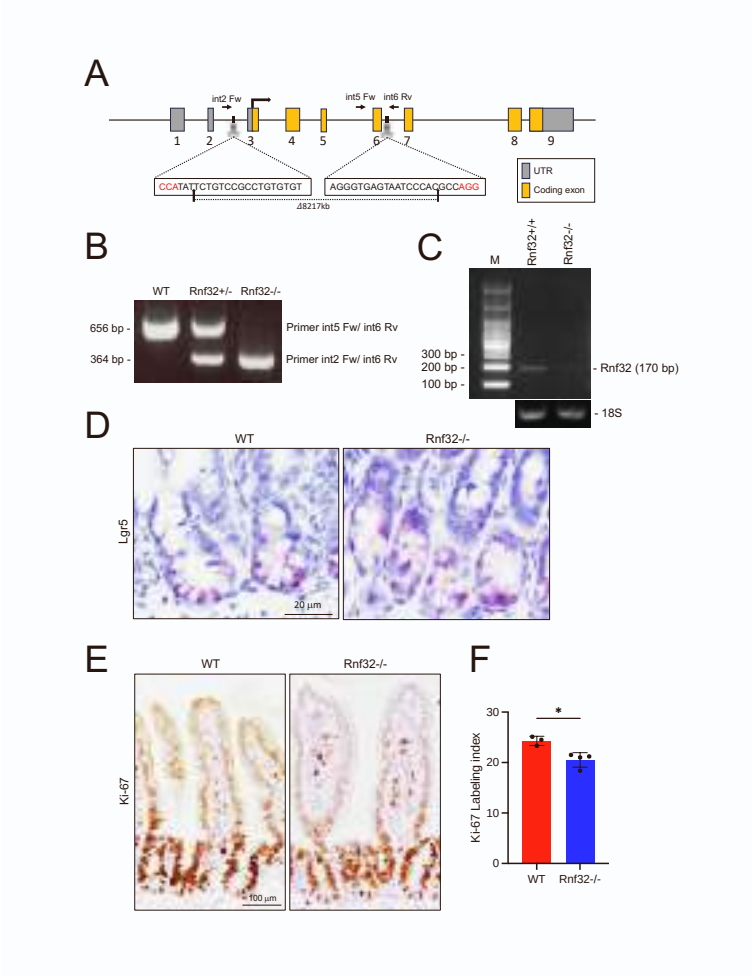

Figure S8: Generation and characterization of Rnf32 knockout mice, related to Figure 6.
(A) Schematic overview of the strategy used to generate the Rnf32 knockout mice. Targeted regions in the mouse Rnf32 locus for genome editing are depicted, with the PAM sequence highlighted in red. The PCR primers (int2 Fw, int5 Fw, and Int6 Rv) used for genotyping are indicated.
(B) Genomic PCR analysis was performed to genotype all progeny.
(C) RT-PCR analysis of Rnf32 expression in colon tissues from Rnf32+/+ and Rnf32-/- mice.
(D) Representative images of Lgr5 ISH on paraffin-embedded sections of small intestines from wild-type and Rnf32-/- mice (n = 3 per group). Scale bars: 20 µm.
(E) Representative images of Ki-67 IHC on paraffin-embedded sections of the small intestine from WT and Rnf32-/- mice (n = 3 per group). Scale bars: 100 µm.
(F) Quantification of the Ki-67 labeling index per crypt. The percentage of Ki-67+ cells per crypt was measured. *$p < 0.05$ (unpaired t-test). Error bars represent s.e.m. n = 3 for WT and n = 4 for Rnf32-/- per group, with 11 and 9 crypts analyzed per WT and Rnf32-/-, respectively.

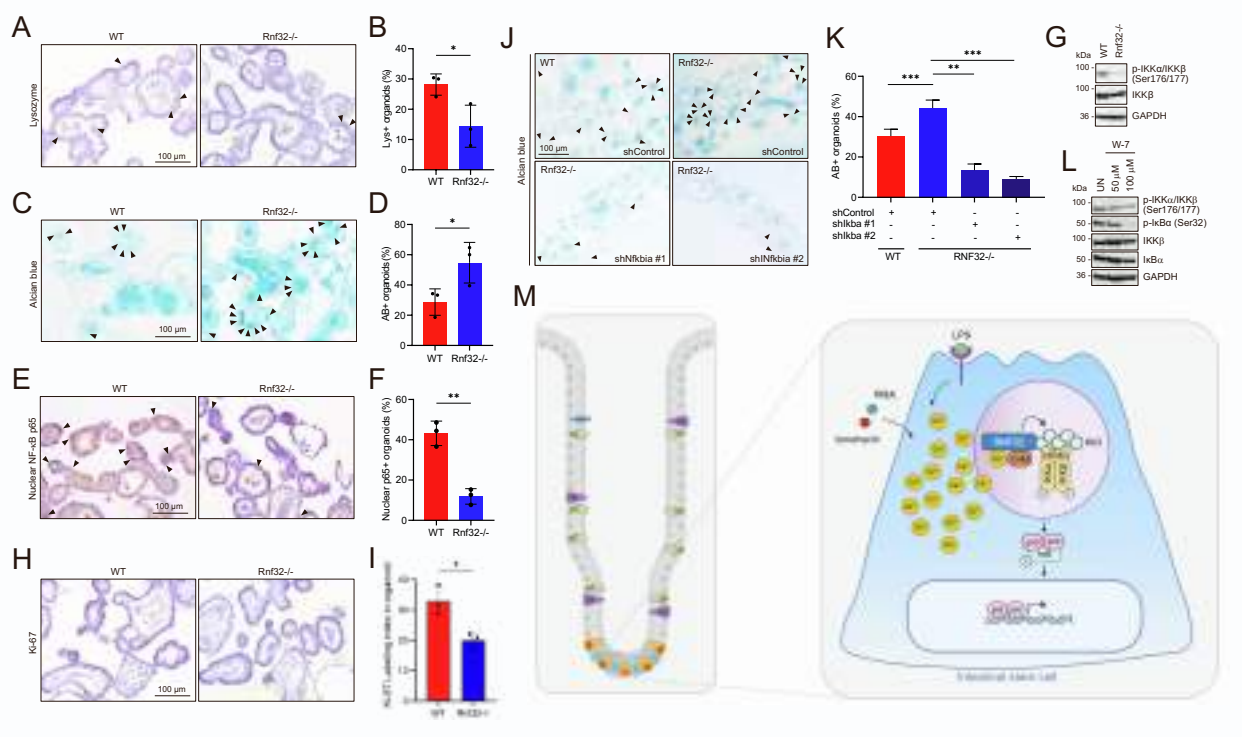

Figure S9: The RNF32-NF-κB axis controls cell fate specification in intestinal organoids, related to Figure 6.

(A) Representative IHC images of staining with anti-lysozyme antibody on paraffin-embedded sections of organoids from the small intestine of WT and Rnf32-/- mice (n = 3 per group). Black arrowheads point to Lys+ Paneth cells. Scale bars: 100 μm.

(B) Quantification of the average percentage of organoid with Lys+ Paneth cells (n = 3 per group with 29, 112, and 90 organoids and 25, 67, and 87 organoids from WT and Rnf32-/- mice, respectively). *p < 0.05 (unpaired t-test). Error bars represent s.e.m.

(C) Representative images of Alcian Blue (AB) staining on paraffin-embedded sections of organoids from the small intestine of WT and Rnf32-/- mice (n = 3 per group). Black arrowheads point to AB^+ goblet cells. Scale bars: 100 μm.

(D) Quantification of the average percentage of organoids with AB+ Goblet cells (n = 3 per group with 24, 140, and 79 organoids and 17, 38, and 60 organoids from WT and Rnf32-/- mice, respectively). *p < 0.05 (unpaired t-test). Error bars represent s.e.m.

(E) Representative IHC images of NF-κB p65 staining on paraffin-embedded sections of the small intestine of WT and Rnf32-/- mice (n = 3 per group). Black arrowheads point to nuclear NF-κB p65 positive cells. Scale bars: 100 μm.

(F) Quantification of the average percentage of organoids with nuclear NF-κB p65-positive cells (n = 3 per group with 35, 112, and 45 organoids and 26, 72, and 71 organoids from WT and Rnf32-/- mice, respectively). **p < 0.01 (unpaired t-test). Error bars represent s.e.m.

(G) Organoids derived from wild-type or RNF32-/- intestines were lysed and analyzed by immunoblotting using antibodies specific to the indicated proteins.

(H) Representative images of Ki-67 staining on paraffin-embedded sections of organoids from the small intestine of WT and Rnf32-/- mice (n = 3 per group). Scale bars: 100 μm.

(I) Quantification of the average percentage of Ki-67 labeling index per organoid. The percentage of $Ki\text{-}67^+$ cells per organoid was measured (n = 3 per group with 19, 8, and 7 organoids and 14, 12, and 8 organoids from WT and Rnf32-/- mice, respectively). *p < 0.05 (unpaired t-test). Error bars represent s.e.m.

(J) Representative images of Alcian Blue staining on paraffin-embedded sections of organoids from the small intestine of WT and Rnf32-/- mice (n = 3 per group) treated with the indicated shRNA.

(K) Quantification of the average percentage of AB^+ organoids (n = 3 per group). **p < 0.01, ***p < 0.001 (unpaired t-test). Error bars represent s.e.m.
(L) Organoids derived from wild-type intestines were treated with the CaM inhibitor W-7 at the indicated concentrations for 120 minutes or left untreated. Organoids were then lysed and analyzed by immunoblotting using antibodies specific for the indicated proteins.
(M) Working model. Created with BioRender.com. See text for description.